DOI:
10.1126/sciimmunol.adl1903

Document Version
Peer reviewed version

The magnitude of adaptive type-2 immunity is locally constrained via a Gata3^{high} Treg – ILC2 axis

Julie Stockis[1,‡], Thomas Yip,[1,‡], Julia Moreno-Vicente[1,‡], Oliver Burton[2], Youhani Samarakoon[1], Shwetha Raghunathan[1], Celine Garcia[1], Weike Luo[1], Sarah K Whiteside[3], Shaun Png[1], Charlotte Simpson[1], Stela Monk[1], Ashley Sawle[1], Kelvin Yin[1], Johanna Barbieri[1], Panagiotis Papadopoulos[1], Hannah Wong[4], Hans-Reimer Rodewald[5], Timothy Vyse[6], Andrew NJ McKenzie[7], Mark S Cragg[8], Matthew Hoare[1,9], David R Withers[10], Hans Jörg Fehling[11], Rahul Roychoudhuri[3], Adrian Liston[2] and Timotheus YF Halim[1,].*

[1] University of Cambridge, CRUK Cambridge Institute, Cambridge, CB2 0RE, UK.

[2] Immunology Programme, The Babraham Institute, Cambridge, CB22 3AT, UK.

[3] Department of Pathology, University of Cambridge, Cambridge, CB2 1QP, UK.

[4] Department of Veterinary Medicine, University of Cambridge, Cambridge, CB3 0ES, UK.

[5] Division of Cellular Immunology, German Cancer Research Center, Heidelberg, Germany.

[6] Department of Medical and Molecular Genetics, King's College London, London SE1 9RT, UK.

[7] Medical Research Council, Laboratory of Molecular Biology, Cambridge, CB2 0QH, UK.

[8] Antibody and Vaccine Group, Centre for Cancer Immunology, School of Cancer Sciences, Faculty of Medicine, University of Southampton, Southampton, SO16 6YD, UK.

[9] University of Cambridge, Department of Medicine, Cambridge CB2 0QQ, UK.

[10] University of Birmingham, Institute of Immunology and Immunotherapy, Birmingham B15 2TT, UK.

[11] Institute of Immunology, University Hospital, Ulm, Germany.

[‡] equal contributions.

Corresponding author:

[*] Tim.Halim@cruk.cam.ac.uk

Summary

Regulatory T cells (Tregs) are essential for limiting adaptive immunity and restrain type-2 inflammation in allergic disease. As Tregs function locally, the mechanisms that coordinate their suppressive role in the inflamed niche are of great interest. Here we show that group 2 innate lymphoid cells (ILC2) are critical orchestrators of Treg cell function. ILC2-derived OX40L and OX40 on Tregs promote the local expansion of Gata3^{high} Tregs, which possess distinct transcriptional and functional programmes that enforce co-localisation with ILC2 in the inflamed airways. Using OX40 Treg-conditional mutant mice, we show that Gata3^{high} Tregs are important for restraining adaptive type-2 immunity. Mechanistically, Gata3^{high} Tregs modulate OX40L bioavailability on ILC2, which controls effector memory Th2 cell formation. As such, ILC2 can simultaneously engage both the effector and regulatory arms of adaptive type-2 immunity via the OX40L-OX40 signalling axis. Hence, ILC2-Treg interactions serve as a critical feedback mechanism to control adaptive type-2 immunity.

Introduction

Unlike epithelial or mesenchymal cells, whose cellular densities are constrained by the structural boundaries of tissues, immune cell densities are largely dictated by local inflammatory mediator or mitogen abundances[1]. As such, inflamed organs can rapidly and profoundly increase immune cell numbers; while this capacity evolved to counter pathogens, concomitant regulatory mechanism are equally important to maintain a fine balance between protective and destructive inflammation. Regulatory T cells (Tregs) are centrally involved in this homeostatic process, although many questions persist about how diverse Treg subsets locally curtail different types of inflammation[2].

Treg deficiencies or depletion often result in unrestrained type-2 inflammation[3–5], although it remains unclear if specific Treg subsets are elicited to suppress CD4$^+$ T helper type-2 (Th2) cells. Shared transcription factors between Tregs and Th2 cells, such as *Irf4*[6] and *Gata3*[7] are important for Treg function in models of type-2 inflammation; however, Treg-specific deletions of these transcription factors are confounded by their graded or low constitutive expression, and concomitant homeostatic or developmental roles. Nevertheless, it is likely that conserved transcriptional machinery promotes co-localisation of effector Th2 cells and Tregs in the type-2 inflamed niche, although this paradigm is better defined for type-1 or type-17 inflammation[8–10]. Relatedly, regulatory-to-effector T cell ratios strongly influence local control of allergic inflammation[11]; moreover, while allergenic peptides underpin pathogenic Th2 cell-driven

inflammation, less is known about the mechanisms that guide Treg-mediated restraint of adaptive type-2 immunity[12,13].

Epithelial or stromal cell sensing of tissue stress initiates type-2 immune activation via the release of interleukin (IL)-33, which acts on both innate and adaptive type-2 immune cells expressing its receptor ST2. While IL-33 strongly promotes type-2 immunity, it also mediates the suppressive functions of ST2$^+$ regulatory Tregs[14,15], and organ-homeostatic roles of ST2$^+$ tissue-resident Tregs[16–18]. While IL-33 can directly influence ST2$^+$ Treg function, other reports suggest that indirect effects of IL-33 guide the overall Treg response[19–21]. Specifically, we showed that expression of the co-stimulatory ligand OX40L (*Tnfsf4*) by ILC2 is critical for simultaneous Th2 and Treg expansion in type-2 inflammation. It remains uncertain if OX40 expression by Tregs is required for their local expansion, and, more importantly, why ILC2 can simultaneously engage Th2 cell-driven effector and regulatory immunity.

Using spatial, cellular and molecular profiling of the type-2 inflamed niche, we found that both Th2 and Gata3^{high} Tregs closely associated with ILC2. Notably, Gata3^{high} Tregs were greatly enriched in type-2 inflammation due to multifaceted ILC2-Treg dialogue involving CCL1-CCR8 and OX40L-OX40 signalling. Unbiased profiling of OX40L expressing cells using a gene-reporter identified ILC2 as the major cellular source in both the type-2 inflamed lung and its draining lymph node. Using OX40 Treg-conditional knockout mice, we found that Gata3^{high} Treg expansion was greatly impaired in response to IL-33-driven allergic inflammation, and moreover, resulted in the profound local expansion of type-2 immune cells. Mechanistically, we found that Gata3^{high} Tregs can directly modulate OX40L surface expression on ILC2; the increased bioavailability of this co-stimulatory molecule in OX40 Treg-deficient mice underpinned unrestrained expansion of memory Th2 cells in the lung and associated lymph-nodes. Thus, ILC2 serve as a critical local orchestrator of Treg-mediated constraint of adaptive type-2 immunity.

Results

The inflamed type-2 immune niche is typified by Gata3^{high} innate and adaptive lymphocytes that possess both effector and regulatory functions.

Both innate and adaptive type-2 effector lymphocytes depend on the transcription factor Gata3 for their development and function. Gata3 can also be expressed by Tregs, and Gata3^{high} Tregs are greatly amplified alongside Gata3^{high} Th2 and ILC2 in the lungs after exposure to IL-33 (Figure 1a, Supplemental Figure 1a). Focussing on Gata3^{high} Tregs, we observed that this

subset was largely CD62L^{-}CD44^{+} and highly expressed KLRG1, a marker associated with tissue-resident Tregs (Figure 1a, Supplemental Figure 1b). By intravenous administration of anti-CD45.2 mAb we confirmed that Gata3^{high} KLRG1^{+} Tregs showed increased tissue-residency compared to Gata3^{low} KLRG1^{-} Tregs, while lung ILC2 were almost exclusively tissue-resident (Supplemental Figure 1c). Next, using multiplex IF microscopy of lung sections we identified CD3^{+}Foxp3^{+} Tregs, CD3^{+}Gata3^{+}Foxp3^{+} Th2 cells, and CD3^{-}Gata3^{+} ILC2 (Figure 1b) after IL-33 administration. Image analysis indicated that Treg and Th2 cells localised closer to ILC2 than CD3^{+}Gata3^{-}Foxp3^{-} conventional T (Tconv) cells (Figure 1c). We also used 2-photon microscopy of anti-CD4 injected *Il5^{tdTom}Foxp3^{YFP}* mouse lung explants to show that ILC2 and Tregs co-localise in the lung adventitial regions after IL-33 administration (Figure 1d). Hence, we hypothesized that both effector and regulatory Gata3^{high} lymphocytes enact transcriptional programmes that enforce their co-localization, and potential dialogue, in the type-2 inflamed niche.

To isolate innate and adaptive type-2 lymphocytes we used *Gata3^{YFP}* reporters (which retain endogenous *Gata3* expression[22]) to generate *Gata3^{YFP}Foxp3^{RFP}* mice (Figure 1e, Supplemental Figure 1d-f). We could accurately identify distinct Gata3^{high} CD4^{+} T cell-types and ILC2, which all expanded in the lung after intranasal IL-33 administration; using flow-sorting we purified these and Gata3^{low} Treg and CD4^{+} Tconv cell subsets for bulk RNA-seq analysis.

Transcriptomically, we found that ILC2, Tregs, Th2 and Tconv cells expressed their respective lineage-associated genes (Figure 1f). Reassuringly, *Gata3* expression levels matched that of the reporter; moreover, Th2 cells and Gata3^{high} Tregs expressed high transcript levels of *Tnfsf4* (OX40), *Klrg1* and *Cd44*, while *Sell* (CD62L) was amplified in Gata3^{low} Tregs and Tconv cells, matching our flow-cytometry data. Interestingly, Th2 as well as Gata3^{high} and Gata3^{low} Tregs expressed both *Ccr4* and *Ccr8*, which are important for Treg and Th2 cell migration into the type-2 inflamed niche[23–25]; notably, Gata3^{high} Tregs expressed more *Ccr8* transcript and surface protein compared to the other subsets (Figure 1g). Moreover, *Ccr7* expression was low on Gata3^{high} Tregs, while Gata3^{low} Tregs and Th2 cells expressed intermediate levels compared to Tconv cells; this may indicate a reduced ability of Gata3^{high} Tregs to traffic to the mediastinal lymph-node (medLN) via lymphatics. Furthermore, Gata3^{high} Tregs, Th2 cells and ILC2 all selectively expressed *Cxcr6*, which is associated with retention of lymphocytes in the tissue-niche[26]. Thus, while all Treg and Th2 cells possess receptors to enter the type-2 inflamed lung niche, Gata3^{low} Tregs do not highly express genes required for retention in the lungs; conversely, Gata3^{high} Tregs (and Th2 cells to a lesser degree) possessed a stronger gene-signature related to tissue-residency (Supplemental Figure 1g).

We next performed TCR diversity analysis on the sorted T cell populations. We found that Gata3^{high} Tregs exhibited significantly reduced TCR diversity and increased proportions of hyper-expanded clones compared to Gata3^{low} Treg and Tconv cells (Figure 1h, Supplemental Figure 1h). Interestingly, Th2 cells of IL-33-treated mice were clonally hyper-expanded, suggesting that endogenous Th2 cells expand in response to local antigen or co-stimulation (Supplemental Figure 1h); indeed, both Gata3^{high} Treg and Th2 cells expressed higher levels of *Nr4a1* (Nur77), indicative of increased TCR stimulation (Figure 1f).

To investigate how type-2 lymphocytes interact in the inflamed niche we performed *in silico* receptor-ligand interactome analysis using CellChat[27] (Figure 1i and j, Supplemental Figure 1i and Table 1). Predicted heterotypic interactions were strongest between ILC2 and Treg or Th2 cells. Interestingly, *Tnfsf4-Tnfrs4* was predicted to preferentially engage Gata3^{high} Tregs while also showing affinity for Gata3^{low} Treg and Th2 cells. Fitting with literature, ILC2 were predicted to engage in multiple autocrine interactions, including via CCL1-CCR8 signalling[28]; interestingly, our results suggested that ILC2 also preferentially engage Gata3^{high} Tregs via this interaction. We used *Ccr8*$^{-/-}$ mice to test if this chemokine axis is important for the IL-33-driven expansion of Gata3^{high} Tregs. While Gata3^{high} Treg numbers were similar in both genotypes at rest, IL-33 administration resulted in impaired expansion of Gata3^{high} Tregs in *Ccr8*$^{-/-}$ mice compared to wild-type control (Figure 1k); notably, a diminished but significant effect of IL-33 in knockout mice suggested that other factors contributed. Moreover, the IL-33-driven increase in ILC2 and Gata3^{low} Treg numbers was not significantly affected by CCR8 deficiency.

These data suggested that ILC2 serve as tissue-resident sentinels that, in addition to Th2 cells, can also rapidly attract and engage Tregs after exposure to the alarmin IL-33. Moreover, while chemokines are important, it is likely that other co-stimulatory ligand-receptor interactions contribute to the local expansion of Gata^{high} Tregs.

ILC2 orchestrate IL-33-dependent expansion of tissue-resident Gata3^{high} Tregs in diverse anatomical sites.

IL-33 has a profound effect on the local expansion and maintenance of Tregs in different organs and tissues, however, it remains unclear if this is due to direct IL-33 signalling. To address this question, we generated mixed bone marrow chimeras using congenic *Il1rl1*$^{-/-}$ and CD57Bl/6 wild-type donors (Figure 2a, Supplemental Figure 2a). Interestingly, we found no substantial effect on Treg cell numbers or proportions due to cell-intrinsic loss of the IL-33

receptor in many organs tested, including the lung, but also non-mucosal sites such as the pancreas and adipose tissue. Conversely, IL-33 administration resulted in the rapid expansion of Treg cells in many peripheral sites (Figure 2b). Notably, non-mucosal sites such as the pancreas also exhibited co-localisation of ILC2 and Treg cells rapidly after IL-33 exposure, suggesting that IL-33-responsive ILC2 may coordinate local Treg cell expansion (Supplemental Figure 2b). Like the lungs, IL-33 also induced the rapid and selective expansion of pancreatic Gata3^{high} Tregs, which preferentially expressed KLRG1 and were tissue-resident based on intravenous CD45.2 labelling experiments (Supplemental Figure 2c and d).

To ask if ILC2 are important mediators of local Treg expansion, we used ILC2-deficient *Il7r*$^{Cre/+}$*Rora*$^{fl/fl}$ or *Il7r*$^{Cre/+}$ control mice. Systemic administration of IL-33 induced the rapid expansion of Tregs in most anatomical sites of control mice, however, ILC2-deficient animals were significantly impaired (Figure 2c). These results demonstrated that the effect of IL-33 on local Treg cell expansion in many anatomical sites is orchestrated by ILC2.

It is known that co-stimulatory ligands can influence local ILC2-Treg cell interactions, including ICOSL and OX40L[19,20]. We therefore generated ICOSL- or used OX40L-conditional mutants where these co-stimulatory molecules were deleted on ILC2. Interestingly, IL-33 administration to *Il5*$^{Cre/+}$*Icosl*$^{fl/fl}$ or *Il5*$^{Cre/+}$ control mice resulted in similar expansion of Gata3^{high} Tregs in the airways, suggesting that ICOSL-ICOS signalling was not essential (Figure 2d). Conversely, *Il7r*$^{Cre/+}$*Tnfsf4*$^{fl/fl}$ mice showed a significant reduction in Gata3^{high} Treg expansion compared to *Il7r*$^{Cre/+}$ controls in the lung, as we previously reported[19], as well as in the pancreas, omentum and adipose tissue after IL-33 administration (Figure 2d, Supplemental Figure 2e). Moreover, while *Icosl* transcript was elevated in ILC2 (Figure 1f), we did not detect surface ICOSL expression by lung ILC2 after IL-33 administration (Supplemental Figure 2f). Conversely, OX40L expression was rapidly induced on lung ILC2 after IL-33 administration, and preceded the local expansion of Gata3^{high} Tregs, as demonstrated in a time-course experiment (Figure 2e, Supplemental Figure 2g); we observed a similar induction of OX40L on ILC2 in other anatomical sites, including the pancreas (Supplemental Figure 2h). To profile cells for their ability to produce OX40L we used *Tnfsf4*$^{hCD4/+}$ reporter mice, where gene activity is measured instead of transient surface expression of OX40L. We detected robust hCD4 expression on both lung and medLN ILC2 after IL-33 exposure, but none in PBS treated mice (Figure 2f and g, Supplemental Figure 2i); moreover, we did not observe hCD4 expression on other lymphocytes, including lymph-node ILC3, at rest or after IL-33 administration (Figure 2g). We next profiled *Tnfsf4*$^{hCD4/+}$ reporter mice for hCD4 expression on myeloid cells. We did not observe hCD4 expression by myeloid cell-types in PBS or IL-33 treated lungs, including alveolar or interstitial macrophages, granulocytes or dendritic cells (Figure 2h). Notably, we

observed some hCD4 expression by cDC2 in the medLN after IL-33 treatment (Figure 2i). Altogether, these results suggest that the IL-33-ILC2-OX40L axis serves as an innate checkpoint for local Gata3^{high} Treg expansion.

Intrinsic OX40 signalling is required for IL-33-dependent Gata3^{high} Treg expansion.

To investigate if Treg-intrinsic OX40 signalling drove IL-33-mediated expansion we generated Treg-conditional mutants (*Foxp3^{Cre}Tnfrsf4$^{fl/fl}$*, OX40$^{\Delta Treg}$) that efficiently and specifically deleted OX40 on Tregs (Supplemental Figure 3a). OX40$^{\Delta Treg}$ mice were born at Mendelian ratios and were phenotypically unremarkable compared to littermate controls. Detailed histological characterization of these mice revealed a minor increase in colonic immune infiltration (Supplemental Figure 3b-c). Nevertheless, the lungs of OX40$^{\Delta Treg}$ mice were histologically similar to control mice at baseline (Supplemental Figure 4b).

Moreover, while total percentages of Tregs were slightly higher in the spleen, the number and percentage of Gata3^{high} Tregs were similar at baseline in the lungs and pancreata of OX40$^{\Delta Treg}$ compared to *Foxp3^{Cre}* control mice, arguing against a substantial role for OX40 in tissue Treg maintenance (Supplemental Figure 3d). We performed *in vitro* suppression assays of flow-sorted splenic Tregs from *Foxp3^{Cre}* control or OX40$^{\Delta Treg}$ mice, which showed that OX40-deletion does not impair their suppressive function (Supplemental Figure 3e). These results were reinforced by transcriptomic analysis of control and OX40-knockout Tregs, which showed that besides *Tnfrsf4*, the Treg transcriptome was largely unaffected at baseline, including *Il1rl1* transcript or surface ST2 expression (Supplemental Figure 3f-g).

Next, we treated OX40$^{\Delta Treg}$ or control mice with IL-33 or PBS followed by immune-phenotyping of different organs; IL-33-mediated expansion of Gata3^{high} Tregs was significantly reduced in the pancreas and spleen, while the proportion of Gata3^{high} Treg was substantially impaired in both the pancreas, lung and spleen (Figure 2j, Supplemental Figure 3h). Hemizygous female *Foxp3$^{YFP\text{-}Cre/+}$Tnfrsf4$^{fl/fl}$* mice were used to further control for cell-extrinsic effects on IL-33-mediated Treg expansion (Supplemental Figure 3i); we found that YFP^{-} OX40-sufficient Tregs expand, while YFP^{+} OX40-knockout Tregs fail to respond to IL-33 administration. Lastly, we generated *Foxp3^{CreERT2}Tnfrsf4$^{fl/fl}$* mice to temporally delete OX40 on Tregs. Tamoxifen treatment before IL-33 administration resulted in efficient deletion of OX40, and significantly impaired Gata3^{high} Treg expansion in the lung and pancreas, similar to the constitutive knock-out (Figure 2k, Supplemental Figure 3j). In all, these data demonstrate a critical Treg cell-intrinsic role of OX40 for mediating IL-33-driven Gata3^{high} Treg expansion in diverse anatomical locations.

Treg-intrinsic OX40 is critical for the effective control of type-2 immunity.

As Treg-intrinsic loss of OX40 selectively impairs the expansion of Gata3^{high} Tregs, which efficiently restrain type-2 immunity[29], we hypothesized that OX40$^{\Delta Treg}$ mice would fail to control IL-33-driven type-2 pathologies. We intranasally sensitized and challenged OX40$^{\Delta Treg}$ and control mice with *Alternaria alternata* fungal allergen extract or PBS control on days 0, 1 and 14, followed by analysis for airway inflammation on day 20. While allergen exposure provoked a robust type-2 immune response in control mice, OX40$^{\Delta Treg}$ mice experienced profound eosinophil-rich allergic lung inflammation (Figure 3a, Supplemental Figure 4a). Moreover, we observed a significant increase in medLN eosinophil numbers in allergen challenged OX40$^{\Delta Treg}$ over control mice. Similarly, while sensitization and challenge induced effector Gata3^{high} Th2 cell expansion in control mice, OX40$^{\Delta Treg}$ mice experienced more than a two-log increase in numbers (Figure 3b). Similarly, ILC2 numbers were increased in inflamed OX40$^{\Delta Treg}$ mice, while no significant or only minor changes were observed in alveolar macrophage and neutrophil numbers (Figure 3c and d). Next, as a measure of lung function, we quantified breadth distention and blood oxygenation on three days following the last allergen challenge (Figure 3e); while control mice experienced only minor changes in these parameters after allergen challenge, we observed a notable and persistent increase in breathing effort and reduced blood oxygenation in OX40$^{\Delta Treg}$ mice. Histological analysis of lungs on day 20 indicated that untreated mice of both genotypes did not exhibit inflammation, however allergen treated OX40$^{\Delta Treg}$ mouse lungs were substantially more inflamed compared to control animals (Figure 3f, Supplemental Figure 4b). Next, we used the protease allergen papain as an alternative model of type-2 airway inflammation. Using a similar dosing scheme, we find that OX40$^{\Delta Treg}$ mice experienced significantly more type-2 inflammation, as assessed by quantification of lung ILC2 and Th2 cells and/or eosinophils in the lung, bronchoalveolar lavage and medLN (Figure 3g). In all, we conclude that OX40 expression by Tregs is critical for restraining airway type-2 inflammation after allergen exposure.

Allergen exposed OX40$^{\Delta Treg}$ mice have impaired Gata3^{high} Treg induction and uncontrolled effector memory Th2 cell expansion.

Inhaled allergens promote IL-33 release, which is essential for both ILC2 activation and subsequent Th2 cell responses[30–33]. Given that this pathway also engages Gata3^{high} Tregs we assessed the lungs of *Foxp3^{Cre}* control and OX40$^{\Delta Treg}$ mice after *Alternaria alternata* challenge by flow cytometry (Figure 4a, Supplemental Figure 5a). Gating on CD44^{+}CD62L^{-} T cells, we find a significant enrichment of Gata3^{high} Tregs in control animals (Figure 4b); concurrently,

Gata3^{high} Treg proportions are significantly reduced in OX40$^{\Delta Treg}$ compared to control mice after allergen exposure. Conversely, the percentage of lung CD44^{+}CD62L^{-} effector Th2 cells is significantly increased in OX40$^{\Delta Treg}$ mice (Figure 4c). Notably, total leukocyte numbers are profoundly increased in allergen treated OX40$^{\Delta Treg}$ mice compared to control animals, resulting in overall increased Gata3^{low} and Gata3^{high} Treg numbers (Supplemental Figure 5b). However, when we compared the ratio of Th2 to Treg cells we observe that while control mice have constant ratios in naïve and inflamed lungs, OX40$^{\Delta Treg}$ mice failed to maintain an equilibrium, resulting in significantly higher effector Th2 to regulatory T cell proportions (Figure 3d). We next used multiplex IF microscopy and HALO image analysis to determine the densities of ILC2, Treg and Th2 cells in the lungs of *Alternaria alternata* challenged *Foxp3^{Cre}* control and OX40$^{\Delta Treg}$ mice (Figure 4e and f). Mirroring flow-cytometric data, we found that OX40$^{\Delta Treg}$ mouse lungs showed increased overall cell densities, and a marked increase in Th2 cell to Treg proportions compared to allergen-treated control mice (Figure 4g). Next, using the protease allergen papain, we also observed an impaired relative expansion of Gata3^{high} Tregs in OX40$^{\Delta Treg}$ mice and amplified Th2 cell expansion, resulting in significantly higher Th2 cell to Gata3^{high} Treg ratios in the lung (Figure 4e-g, Supplemental Figure 5c). These data support our hypothesis that OX40-driven co-expansion of Tregs is important for the restraint of Th2 cell numbers during inflammation.

Given the importance of secondary lymphoid organs for generating both effector and memory Th2 cell responses, we next focussed our attention on the medLN (Figure 4h). Unlike the lung, we did not observe significant changes in the proportion of Gata3^{high} or total Treg percentages after allergen challenge or between genotypes (Figure 4i, Supplemental Figure 5d). However, the percentage of Th2 cells increased upon allergen challenge in control mice, and this was significantly amplified in OX40$^{\Delta Treg}$ mice (Supplemental Figure 5e). We then assessed Th2 cells for the presence of CD44^{+}CD62L^{-}CD127^{+} effector memory cells (Figure 4j), and found that allergen sensitized OX40$^{\Delta Treg}$ mice showed a significant increase in the percentage and absolute numbers of effector memory Th2 cells compared to control animals (Figure 4k and l). Using papain allergen, we found a similar significant increase in the percentage of effector memory Th2 cells in the medLN of OX40$^{\Delta Treg}$ mice (Figure 4m). Hence, we conclude that OX40 deficiency on Tregs results in a greatly amplified memory Th2 cell response in the lung-draining lymph node.

Gata3^{high} Tregs directly control OX40L availability and preferentially home to the inflamed lung.

Given the critical role of OX40L-OX40 signalling on the control of T cell memory[34], and ability of Tregs to control the surface expression of co-stimulatory ligands[2], we hypothesized that Tregs may modulate OX40L bioavailability on lung ILC2. Utilizing *Foxp3*^{DTR} mice, we asked if acute Treg depletion could influence OX40L expression upon IL-33 stimulation. Indeed, we observed a significant increase in the percentage and mean fluorescence intensity of OX40L on ILC2 in IL-33 plus diphtheria toxin treated mice (Figure 5a and b). Concomitant analysis of myeloid cell-types indicated that Treg depletion did not influence OX40L surface expression on granulocytes, or macrophage and dendritic cell subsets in IL-33 treated mice (Figure 5c).

We next employed an *in vitro* co-culture system to assess the ability of Tregs to regulate OX40L expression on ILC2 (Supplemental Figure 6a). We used *Gata3*^{YFP}*Foxp3*^{RFP} mice to purify viable lung Gata3^{high} and Gata3^{low} Tregs, as well as Gata3^{high} ILC2 (Figure 5d). Culture of ILC2 with IL-33 resulted in expression of OX40L, which was significantly reduced upon co-culture with Gata3^{high} Tregs, while Gata3^{low} Tregs showed reduced capacity to suppress OX40L expression (Figure 5e and f). Importantly, we did not detect OX40L on the surface of Tregs *in vivo* after IL-33 administration or *in vitro* after co-culture with ILC2, arguing against trogocytosis-mediated suppression (Figure 5a and e); moreover, we confirm that *Gata3* expression patterns were maintained by Tregs in culture (Supplemental Figure 6b).

We subsequently investigated the mechanism whereby Tregs modulate OX40L expression by ILC2. First, we found that *Tnfsf4* transcript levels were unchanged after co-culture with Tregs, arguing against transcriptional regulation (Supplemental Figure 6c). We also failed to detect soluble OX40L in co-cultures, suggesting that cleavage of membrane-bound receptors did not account for loss of expression (*data not shown*). Next, we focussed on internalization of OX40L; however, we found that while blocking endocytosis using Pitstop 2 increased OX40L surface expression on ILC2 in monocultures, the addition of this reagent did not impact Treg-dependent reductions of OX40L expression in co-culture (Figure 5g). Interestingly, the addition of recombinant IL-10 or TGF-β1 to ILC2 monocultures resulted in a significant reduction in OX40L surface expression; however, blockade of either single or both suppressive molecules in ILC2-Treg co-cultures did not revert suppression of OX40L (Figure 5g). Notably, recombinant IL-10 and TGF-β influenced *Tnfsf4* transcript level (Supplemental Figure 6c), indicating a different mechanism of control. Moreover, we sorted Tregs from OX40$^{\Delta Treg}$ mouse lungs which were able, but less-effective than Gata3^{high} Tregs at suppressing OX40L on ILC2 (Figure 5f); while reduced Gata3^{high} Treg numbers in OX40$^{\Delta Treg}$ mouse lungs likely contributed to this result, it also demonstrated that the regulation of OX40L on ILC2 could occur independent of receptor-ligand engagement. This finding was further substantiated using anti-OX40 mAb in co-cultures, which did not affect OX40L suppression by Tregs (Figure 5g).

We used computational tools to explore alternative regulatory mechanisms. First, we analysed predicted Treg-to-ILC2 communication, focussing on modules enriched in Gata3^{high} Tregs (Figure 5g, Table 2). These included adhesion molecules (*Vcam*, *Icam*, *Lamc1*, and *Lgals9*) and the ATP hydrolase CD39 (*Entpd1*), amongst others. Interestingly, IL-10 and TGF-β signalling pathways were not predicted, although this matched our *in vitro* results, and may reflect the lack of TCR stimulation of the Tregs in our setting. Secondly, we compared relative gene expression of known or putative regulatory mechanisms employed by Tregs in our dataset (Figure 5k). Besides the secreted factors already investigated, we found that Gata3^{high} Tregs expressed *Fgl2*, although this was also highly expressed by ILC2 themselves, as well as *Ebi3* which together with *Il12a* forms IL-35. In terms of inhibitory surface molecules *Pdcd1lg2* (PD-L2) was highly expressed by both Gata3^{high} Tregs and ILC2, while the soluble of membrane molecule *Cd83* (CD83) was selective for the former. Gata3^{high} Tregs also selectively expressed *Il2ra*, *Il1r2* and *Il1rl1*, which may act to inhibit IL-2 or IL-33 signalling. Lastly, surface enzymes including *Entpd1* and *Nt5e* (CD73) were expressed by Gata3^{high} Tregs, indicating that adenosine mediated signalling could contribute to reduced OX40L expression by ILC2.

Lastly, as ILC2-Treg co-localisation likely underpins their regulatory function, we asked if Gata3^{high} Tregs preferentially home to the inflamed lung. We adoptively transferred equal numbers of lung Gata3^{high} and Gata3^{low} Tregs into IL-33-treated *Rag2*$^{-/-}$ recipient mice, which lack T and B cells but have lung ILC2, followed by quantification of Tregs in the lungs and spleen (Figure 5g, Supplemental Figure 6d). We observed significantly more Gata3^{high} Tregs in the lung, while equal but greatly reduced numbers of Gata3^{high} and Gata3^{low} Tregs were recovered in the spleen. Moreover, we find that adoptively transferred Tregs maintained their *Gata3* expression pattern (Supplemental Figure 6e). In summary these data showed that airway Gata3^{high} Tregs are endowed to traffic to the inflamed lung niche, while also possessing enhanced capacity for regulating OX40L expression on ILC2.

OX40^{+} Tregs control adaptive type-2 immunity by modulating OX40L availability.

Our data advance a paradigm whereby OX40-expression on Tregs is important for their local expansion and modulation of OX40L expression by ILC2. Increased OX40L availability in the absence of regulation by Gata3^{high} Tregs may therefore explain unrestrained effector memory Th2 cell formation in OX40$^{\Delta Treg}$ mice. To test this hypothesis we used two approaches; first we asked if we could restore Th2 cell-driven allergic inflammation in OX40L$^{\Delta ILC2}$ mice using an OX40 agonist (Supplemental Figure 7a). As expected, OX40L$^{\Delta ILC2}$ mice failed to mount an

efficient Th2 cell response to inhaled allergen papain (Figure 6a). Agonistic murine IgG1 anti-OX40 administration led to the restoration of both airway Th2 cell responses and increased type-2 inflammation, while also promoting a trend towards more Gata3^{high} Tregs. In the medLN, OX40-agonist treatment reversed the defect in effector memory Th2 cell formation observed in OX40L$^{\Delta ILC2}$ mice and rescued the absolute numbers of Th2 cells (Figure 6b). Next, we asked if increased OX40L availability was responsible for unrestrained Th2 cell-driven inflammation by neutralizing OX40L in OX40$^{\Delta Treg}$ mice (Supplemental Figure 7b). As expected, OX40$^{\Delta Treg}$ mice treated with papain allergen exhibited amplified type-2 airway inflammation and Th2 cell numbers, while Gata3^{high} Treg expansion was impaired (Figure 6c); anti-OX40L treatment of OX40$^{\Delta Treg}$ mice significantly reduced type-2 inflammation and airway Th2 cell numbers. Notably, we found no additive effect of OX40L-neutralization on Gata3^{high} Treg enrichment in OX40$^{\Delta Treg}$ mice. More strikingly, we found that OX40L neutralization reverted the amplified CD127^{+} effector memory Th2 cell phenotype observed in mLN of OX40$^{\Delta Treg}$ mice (Figure 6d and e), which resulted in significant reductions in effector memory Th2 cell percentages and numbers, and an overall reduction in Th2 cells (Figure 6e). Histological analysis of the lungs further indicated that overt allergic inflammation observed in OX40$^{\Delta Treg}$ mice after allergen exposure was reduced by anti-OX40L treatment (Figure 6f). Lastly, we leveraged 2W1S peptide-specific tetramers to better understand the effect of Treg-derived OX40, and OX40L-neutralization, on the clonal dynamics of Th2 cells. Papain plus 2W1S peptide administration resulted in the expansion of 2W1S:tetramer^{+} CD4^{+} T cells, which were skewed towards a Gata3^{+} Th2 cell fate (Figure 6g). Mirroring total Th2 cell results, we found that OX40$^{\Delta Treg}$ mice treated with papain plus 2W1S peptide had significantly more 2W1S:tetramer^{+} Th2 cells, which were reduced with neutralization of OX40L (Figure 6g). Overall, these data support our hypothesis that OX40L availability is tuned by OX40^{+} regulatory T cells; this mechanism controls the magnitude of adaptive type-2 immunity by regulating immune memory formation.

Discussion

Local immune-regulatory mechanisms are fundamentally important for maintaining or restoring tissue-homeostasis. Our data advance a paradigm whereby innate lymphoid cells are critical immune-regulatory hubs that locally establish immune tolerance or immune restraint. We demonstrate that OX40L expression by ILC2 is crucial for local co-expansion of both effector and regulatory arms of adaptive type-2 immunity. Using a combination of OX40L and OX40 conditional knockout mice, we illustrate how tissue-resident ILC2 are centrally involved in orchestrating Treg-mediated restraint of adaptive type-2 inflammation in the airways; these data reconcile the recognized role of OX40 for Th2 cell memory formation with its ambiguous function on Tregs[36]. Moreover, we show that ILC2-driven expansion of Gata3^{high} Tregs and

Th2 cells are underpinned by distinct regulatory modules that support migration into the inflamed airway niche. In all, this work provides a novel framework that illustrates how adaptive type-2 immunity is locally regulated and controlled by innate lymphoid cells.

Extending from our previous observation that ILC2 promote Treg expansion[19], we now show that the potent effects of IL-33 on local Treg expansion are dependent on ILC2 and its reliance on the OX40L-OX40 signalling axis in various anatomical locations. Notably, *Icosl* deletion in ILC2 did not significantly impair IL-33-driven Treg expansion, although it remains possible that ILC2-derived ICOSL can influence other aspects of ICOS$^+$ Treg biology. Moreover, Treg-conditional OX40 knockout mice provide compelling proof that intrinsic OX40 signalling is required for IL-33-driven expansion; cell-extrinsic influences are further excluded using female heterozygous *Foxp3*$^{Cre/+}$ mice. These data confirm assertions made using OX40L conditional knockout mice and full-body OX40 knockout animals[19], where Treg-extrinsic effects could not be excluded; moreover, we reconcile similar observations made in ST2 conditional knockout mice treated with IL-33[21] and our own ST2 knockout mixed bone marrow chimera experiments. Hence, the profound effect of IL-33 on tissue-resident Treg expansion is largely due to ILC help. It is likely that OX40L expression by other immune cells, including ILC3, plays an important role on Treg biology in other anatomical sites[37], or under alternative inflammatory conditions where ILC2 are not engaged[38]. Conversely, intestinal ILC3 rely on antigen presentation for generating Treg-dependent peripheral tolerance to microbial antigens[39], whereas ILC2 do not express MHCII in the airways. Nevertheless, TCR engagement is crucial for both Th2 and Treg activation and it is likely that another MHCII$^+$ cell-type locally contributes to the ILC2-Treg immune axis. Indeed, we know that ILC2 interact with dendritic cells in the airways after allergen-driven IL-33 release[31,40], although we have not investigated potential interactions that involve DCs in this study. However, our *Tnfr4*$^{hCD4/+}$ mouse results indicate that both lung and medLN ILC2 are the major cell-type expressing *Tnfsf4* during acute IL-33-driven inflammation. Collectively, our data expand on previous ILC2-Treg interaction results[19,20], and the emerging appreciation of ILC3-Treg crosstalk in the gut[37,39,41,42], to advance the concept that innate lymphoid cells are fundamental regulators of Treg biology in the tissue-niche.

Regulatory T cells can acquire transcriptomic signatures that mirror conventional Th1, Th2 or Th17 polarization states; there is emerging evidence that shared master transcription factor utilization between effector and regulatory CD4 T cells enforces cooperative homing to the inflamed niche[9,43]. Cellular parity between Treg and effector T cells in the tissue niche is critical for effective control of inflammation[44]. While *Tbx21* (T-bet) and *Rorc* (RORγt) targeted Treg experiments support this framework for Th1 and Th17 cells[8,45,46], *Gata3* conditional mutant mice suffer from more global defects[7,29], likely due to constitutive expression by all Tregs.

Using reporter mice where endogenous *Gata3* expression is retained[22] we flow-sorted Gata3^{high} and Gata3^{low} Tregs for functional and transcriptomic studies. Our transcriptomic profiling shows that Gata3^{high} Tregs represent a lung tissue-resident population (as also demonstrated by our *in vivo* labelling experiments in the pancreas and lung); Gata3^{high} Tregs are clonally expanded in the lungs and highly express genes involved in tissue-residency or homing to the type-2 inflamed niche. We also find that Gata3^{high} Tregs are selectively retained in the lungs of IL-33-treated recipient mice compared to Gata3^{low} Tregs. These data support a growing body of work where Gata3-target genes, such as *Ccr4*[47] or *Il1rl1*[48], mark a population that can selectively antagonize adaptive type-2 immunity[49,50]. Nevertheless, given low baseline expression of Gata3, it is possible that Gata3^{low} Tregs can respond, albeit less efficiently, to type-2 inflammation in the lung. Indeed, uncontrolled type-2 lung inflammation in OX40$^{\Delta Treg}$ mice results in overall Treg infiltration, although there is a specific defect in Gata3^{high} Treg expansion.

We also found that Gata3^{high} Tregs are more efficient at suppressing surface expression of OX40L on ILC2 in co-culture. In conjunction with *in vivo* OX40 agonist and OX40L antagonist experiments, these data indicate that Tregs can tune OX40L bioavailability to effector Th2 cells, which subsequently determines the magnitude of the memory response[34]. How Tregs influence surface OX40L expression on ILC2 remains uncertain, although *in vitro* experiments indicate that IL-10 and TGF-β, trogocytosis or direct competition for OX40L are not responsible.

Our results also provide novel insight into OX40L-OX40 biology. Human genome wide association studies strongly associate this signalling axis with inflammatory diseases, including asthma[51]. Moreover, specific single nucleotide polymorphisms in the upstream region of *TNFSF4* are associated with enhanced expression of OX40L and correlate with systemic lupus erythematosus, allergic rhinitis and asthma[52,53]. Animal and human research has conclusively shown that OX40 is critical for the formation of immunological memory in conventional CD4 T cells[36], and numerous studies have attempted to leverage this axis in both inflammatory disease or cancer settings. Nevertheless, these studies did not appreciate the dualistic role of OX40L-OX40, which may have contributed to the modest clinical efficacy observed to date[54–56].

In summary, our work identifies ILC2 as a central signalling node for both effector and regulatory T cells, and the importance of co-expanded Gata3^{high} Tregs for restraining adaptive type-2 immunity. Hence, ILC2-Treg interactions represent an underappreciated mechanism

that operates in parallel to limit the memory Th2 cell response to allergens. Moreover, we reveal how the essential function of Tregs is locally enforced by innate lymphoid cells.

Acknowledgements

We acknowledge the following funding sources: European Union's Horizon 2020 research and innovation programme under the Marie Skłodowska-Curie grant agreement (PanILC No 840501, JS), The Royal Society and Wellcome Trust (204622/Z/16/Z, TYH), Cancer Research UK (CRUK) core award (A24995, TYH). We thank Prof. Marina Botto for the *Tnfsf4*$^{fl/fl}$ mice. We thank the CRUK-CI research instrumentation, flow cytometry, genomics, bioinformatics, histopathology, microscopy, transgenics and BRU cores for their expertise and help.

Author Contributions

JS designed and conducted experiments, and wrote the manuscript. TY, JMV, OB, SR, CG, WL, SKW, SP, CS, SM, AS, JB, SS, PP, KY and HW assisted with experiments and/or analysis. HR, TV, ANJM, MSC, HJF, MH, DRW, RR and AL provided reagents, data and/or advice. TYH supervised the study, designed and conducted experiments, and wrote the manuscript.

Competing Interests Statement

N/A

Methods

Mice

Foxp3^{DTR} ([57]) (JAX #016958), *Foxp3*$^{YFP\text{-}Cre}$ ([58]) (JAX #016959), *Foxp3*^{CreERT2} ([59]) (JAX #016961), *Foxp3*^{RFP} ([60]) (JAX #008374), *Il5*$^{tdTom\text{-}Cre}$ ([61]) (JAX #030926) were bought from JAX, and were maintained in the Cancer Research UK – Cambridge Institute (CRUK-CI) animal facility, under specific-pathogen-free conditions along with *Il7r*$^{Cre/+}$ (provided by Prof. Rodewald), *Il7r*$^{Cre/+}$*Rora*$^{fl/fl}$, *Il7r*$^{Cre/+}$*Tnfsf4*$^{fl/fl}$ (*Tnfsf4*$^{fl/fl}$ mice[62] provided by Prof. Vyse and Prof. Botto), *Tnfrsf4*$^{fl/fl}$, *Foxp3*$^{YFP\text{-}Cre}$*Tnfrsf4*$^{fl/fl}$, *Foxp3*^{CreERT2}*Tnfrsf4*$^{fl/fl}$, *Gata3*$^{YFP/YFP}$ ([22]) (provided by Prof. Fehling), *Gata3*$^{YFP/YFP}$*Foxp3*^{RFP}, *Il13*^{tdTom} (provided by Prof. McKenzie), *Il13*^{tdTom}*Foxp3*$^{YFP\text{-}Cre}$, *Il5*$^{tdTom\text{-}Cre}$*Foxp3*$^{YFP\text{-}Cre}$ mice, *Il5*$^{tdTom\text{-}Cre}$*Icosl*$^{fl/fl}$ and *Tnfsf4*^{hCD4} all in the CD57BL/6 background. Wild-type C57BL/6J mice were purchased from Charles River. Animal work was conducted under project licenses PD7484FB9 or PF993249 at the CRUK-CI (with approval from the Cancer Research UK - Cambridge Institute, Animal Welfare Ethical Review Body) all in accordance with Home Office regulation. CD45.1 mice and *Il1rl1*$^{-/-}$ mice were maintained in the Medical Research Councils ARES facility (Babraham, UK). *Ccr8*$^{-/-}$ mice were maintained in the Cambridge University Biomedical Services Gurdon Institute animal facility. Experiments involving these strains (all on the C57BL/6 background) were performed in these facilities. Mice were sex and age matched whenever possible, and most mice were used at 8-12 weeks of age.

Tnfrsf4$^{fl/fl}$ mouse generation

The *Tnfrsf4*$^{tm1a(EUCOMM)Wtsi}$ ES cells were purchased from the European Mouse Mutant Cell Repository (EuMMCR, HelmholtzZentrum Munchen, GB) and injected into wild type CD1 8-cell stage embryos. Microinjected embryos were cultured in KSOM +AA media (KCl, enriched simplex optimisation medium with amino acid supplement, Zenith Biotech) at 37^{o}C with 95% humidity and 5% CO_2 until they reached the blastocyst stage. Blastocysts were transferred into pseudopregnant recipients. The resulting F0 mice were bred to C57BL/6 mice, proving germline transmission. Superovulated *Tnfrsf4*$^{(fl/+)}$ female mice were further *in vitro* fertilised by C57BL/6 flp sperm in order to remove the neo-cassette.

Tnfsf4^{hCD4} mouse generation

Stock animals (also known as C57BL/6J-Ox40l^{em1H}/H) were generated by the Mary Lyon Centre at MRC Harwell (MLC) via pronuclear injection of CRISPR/Cas9 reagents into 1-cell stage embryos. The MLC generated this mouse strain as part of its commitment to the Genome Editing Mice for Medicine project funded [MC_UP_1502/3] by the Medical Research Council.

The research reported in this publication is solely the responsibility of the authors and does not necessarily represent the official views of the Medical Research Council.

***In vivo* procedures**

rmIL-33 (0.5 µg, Biolegend), diphtheria toxin (10 ng/g, Sigma), 2W1S peptide (25 µg, Genescript) and anti-OX40L mAb (200 µg, Clone RM134L, BioXcell) were administered by intraperitoneal injection in 200 µl of PBS. Anti-OX40L mAb was treated beforehand with 0.05 units of PNGaseF (Promega V483A) per ug of antibody. Samples were incubated at 37°C overnight and purification of the antibody from the enzyme was achieved through size-exclusion dialysis (Pur-A-Lyzer Maxi Dialysis Kit, Maxi 50000, Sigma-Aldrich). Successful de-glycosylation was confirmed by SDS-PAGE electrophoresis. For intranasal administration, mice were anesthetized by isofluorane inhalation, and received rmIL-33 (0.2 µg, Biolegend), Papain (10-15 µg, Sigma), *A. alternata* (10 µg, Greer Laboratories) or anti-OX40 mAb (40 µg, OX86 mIgG1, Antibody and Vaccine group, University of Southampton) in 40 µl of PBS. For induction of Cre-ERT2–mediated recombination, mice were fed tamoxifen-containing food (TD.55125; Envigo). Labelling of circulating leukocytes to evaluate tissue-residency was achieved by i.v. injection of 3 µg anti-CD45.2-PE (clone 104, Biolegend) antibody 3 min prior to sacrifice.

Mixed bone marrow transplantation

CD45.1 x CD45.2 recipient mice were lethally irradiated (2 doses of 5.5 Gy) followed by intravenous transplantation of 2 x 10^6 bone marrow cells, as a 50/50 mix of CD45.1 and ST2-KO. Mice were given Baytril in drinking water for 3 weeks and used for analysis at 8 weeks post-transplant. 2 µg of anti-CD45-biotin was injected i.v. 3 min prior to sacrifice to label circulating leukocytes.

Pulse oximetry

The right hind legs of mice were shaved using an electric razor and then depilated using hair removal cream before pulse oximetry (MouseOX Plus Pulse Oximeter, STARR Life Sciences Corp., PA, USA). Mice were anaesthetized (3% isoflurane for induction, followed by 1.5% for maintenance, v/v in supplied air) and kept on a warming pad throughout the measurement. Blood oxygenation and breadth distention were recorded using the ThighClip mouse thigh sensor and analysed using MouseOX Plus v1.5 software (STARR Life Sciences Corp., PA, USA).

Histology

Tissues were fixed in 10% neutral buffered formalin and embedded in paraffin before sectioning into 3-µm slices. Sample embedding, sectioning, and hematoxylin and eosin staining were conducted by the CRUK-CI Histology Core. Scoring of the colon and lung sections was done by a board-certified veterinary pathologist blinded to the groups and experimental conditions, as previously described.[63,64]

Single cell preparation

Lung

Cell suspensions were prepared by mechanical dissociation, followed by digest in 4 ml of RPMI-1640 containing collagenase I (563 U/ml) and DNase I (0.225 mg/ml) for 1 hour at 37°C on a shaker (220 rpm), followed by filtration through a 70 µm strainer and red blood cell (RBC) lysis.

Pancreas

Pancreata were weighed, then mechanically dissociated, followed by digest in 5 ml of HBSS containing collagenase I (375 U/ml), DNase I (0.15 mg/ml) and Soybean Trypsin inhibitor (Sigma, 0.05 mg/ml) for 30 minutes at 37°C on a shaker (220 rpm), followed by dissociation on a syringe and needle, filtration through a 70 µm strainer and RBC lysis.

Omentum and Adipose tissue

Tissues were weighed, then digested in 0.5 ml of HBSS containing collagenase I (375 U/ml), DNase I (0.15 mg/ml) and Soybean Trypsin inhibitor (Sigma, 0.05 mg/ml) for 45 minutes at 37°C on a shaker (1100 rpm), followed by filtration through a 70 µm strainer. Strainers were further washed with 10 ml warm RPMI-10%FCS.

Spleen

Spleens were strained through a 70 µm filter in RPMI-1640 before RBC lysis.

Mediastinal lymph node

Cell suspensions were prepared by mechanical dissociation, followed by digest in 0.5 ml of RPMI-1640 containing collagenase I (375 U/ml) and DNase I (0.15 mg/ml) for 45 min at 37°C on a shaker (1100 rpm), followed by red blood cell (RBC) lysis.

BAL

BAL cells and fluid were obtained in 1 ml PBS.

Flow cytometry

Single cells were incubated with anti-mouse CD16/32 (Thermo Fisher) to block Fc receptors. For intracellular staining we used the Foxp3/Transcription Factor Kit (Thermo Fisher). Data was acquired on a BD Fortessa or Symphony instrument. Cells were quantified using CountBright beads. Data was analysed using FlowJo X (Tree Star).

The following antibodies were used in this study, with clones, venders, and fluorochrome as indicated:

CD8 (53-6.7, eBioscience, PerCP-eFluor710), CD45 (30-F11, Biolegend, BV510), NK1.1 (PK136, BD, BUV395), CD4 (RM4-5, eBioscience, AF700), B220 (A3-6B2, eBioscience, APC-eFluor780), CD127 (SB/199, BD, PE-CF594), CD44 (IM7, Biolegend, BV785), CD62L (MEL-14, Biolegend, BV605), OX40L (RM134L, Biolegend, AF647 or eBioscience, PE), OX40 (OX-86, eBioscience, PE), Ccr8 (SA214G2, Biolegend, BV421), KLRG1 (2F1, Biolegend, BV605 or eBioscience, PerCP-eFluor710), ST2 (RMST2-2, eBioscience, PE), TCRβ (H57-597, Biolegend, PE), Gata3 (TWAJ, eBioscience, eFluor660), Foxp3 (FJK-16s, eBioscience, AF488), RorgT (Q31.378, BD, BV650), FceRIa (MAR-1, eBioscience, PerCP-eFluor710), CD172α (P84, Biolegend, AF488), Siglec-F (1RNM44N, eBioscience, SB600), XCR1 (ZET, Biolegend, BV650), CD64 (X54-5/7.1, Biolegend, BV711), CD11b (M1/70, Biolegend, BV785), I-A/I-E (CI2G9, BD, BUV395), CD11c (N418, eBioscience, AF700), F4/80 (BM8, eBioscience, APC-eFluor780), Ly6G (1A8-Ly6g, eBioscience, PE-eFluor610), Ly-6C (HK1.4, eBioscience, PE-Cy7). Lineage cocktail contained either CD5 (53-7.3), CD19 (1D3), CD11b (M1/70), CD11c (N418), FcεR1α (MAR-1), F4/80 (BM8), Ly-6C/G (Rb6-8C5), and Ter119 (TER-119), or CD3 (145-2C11), NK1.1 (PK136), CD5 (53-7.3), CD19 (1D3) and B220 (RA3-6B2), all on eFluor450 (eBioscience). Dead cells were excluded with the fixable viability dye UV455 or eFluor780 (eBioscience).

ILC2 and Treg cell isolation and co-culture

Single cell suspensions from IL-33-sensitised lungs from *Gata3*$^{YFP/YFP}$*Foxp3*^{RFP} mice were used to isolate ILC2s (Live CD45^{+}CD3^{-}CD4^{-}Foxp3$^{(RFP)-}$Gata3$^{(YFP)high}$) and Gata^{high} and Gata^{low} Treg cells (Live CD45^{+}CD3^{+}CD4^{+}Foxp3$^{(RFP)+}$Gata3$^{(YFP)high\ or\ low}$) by flow cytometry using a BD Melody instrument. Purified cells were co-cultured overnight in equal concentrations in RPMI-1640 supplemented with 10% FCS, 100 U/ml penicillin (Gibco), and 100 µg/ml streptomycin (Gibco), along with rmIL-33 (10 ng/ml, Biolegend), rhIL-2 (25 ng/ml, Peprotech) and rhIL-7 (10 ng/ml, Peprotech), and where indicated with additional Pitstop (10 µM, Sigma), rhIL-10 (20 ng/ml, Biolegend), rhTGF-β1 (4 ng/ml, Peprotech), anti-IL10 mAb (20 µg/ml, BioXCell, clone JES5-2A5), anti-IL10R mAb (20 µg/ml, Biolegend, clone 1B1.3a), anti-TGF- β1,2,3 mAb (20 µg/ml, BioXCell, clone 1D11.16.8), or anti-OX40 mAb (20 µg/ml, Antibody and Vaccine group, University of Southampton, clone OX-86). Cells were cultured at 37°C in a humidified, 5% CO_2

incubator for 18 hours, before analysis by flow cytometry, qPCR or detection of soluble OX40L in supernatants.

qPCR analysis for *Tnfsf4*

RNA was extracted with the RNeasy Plus kit (Qiagen), and converted into cDNA using the High-Capacity RNA-to-cDNA Kit (Thermo Scientific), followed by qPCR using the TAKYON Low Rox Probe Master mix dTTP Blue (Eurogentec) and primers/probe pre-designed assays for *Tnfsf4* (Mm.PT.58.6713411) (Integrated DNA Technologies). To avoid misinterpretation due to cell number difference in between ILC2 mono-culture and co-culture with Tregs, *Tnfsf4* Ct values were not normalised to a housekeeping gene, having verified beforehand the absence of *Tnfsf4* transcript in Treg mono-culture. Results are expressed as arbitrary units set to 100 for the expression of *Tnfsf4* in ILC2 mono-culture in each independent experiment.

ELISA analysis for soluble OX40L

Supernatants from ILC2 monocultures or ILC2 plus Treg co-cultures were collected and assessed for soluble OX40L by sandwich ELISA (Thermo Fisher), following manufacturer instructions.

***In vitro* T cell suppression assay**

Assay was carried out according to Collison et al.[65] Briefly, a twofold titration series of FACS-sorted spleen and LN Treg ($CD45^+CD3^+CD4^+CD8^-TCR\beta^+YFP^+$) cells starting from 25,000 cells per well was set up in U-bottom 96-well plates. 25,000 FACS-sorted, CellTrace Violet (Invitrogen)-labelled spleen and LN Tconv ($CD45^+CD3^+CD4^+CD8^-TCR\beta^+YFP^-$) cells were then added to each well, in addition to anti-CD3/CD28 coated beads (Gibco) at a final concentration of 6.25 $x10^4$ beads/ml. Cells were incubated in a final volume of 200 µl IMDM with 10% FBS, 100 U/ml penicillin (Gibco), 100 µg/ml streptomycin (Gibco), 1x Glutamax (Gibco) and 5.5 µM β-mercaptoethanol (Gibco), and incubated in 5% CO2 at 37 °C for 5 days before analysis on a BD FACS Symphony. Results were expressed as described by Hu et al.[66]

Microscopy

For imaging of precision-cut lung slices (PCLS), $Il5^{tdTom/+}Foxp3^{YFP\text{-}Cre}$ mice were injected with 200 ng rmIL-33 intranasally for 2 days. 5 days after the first injection, mice were sacrificed and lungs were inflated with 1 ml of 2% low melting point agarose diluted in PBS. 200 µm sections were prepared using a Leica VT 1200S Automated Vibrating Blade Microtome**.** PCLS were then washed in RPMI supplemented with 10% FCS for 15 min at 37°C. Anti-CD4-AF647 (clone RM4-5, Invitrogen) was prepared in RPMI and lung slices were incubated in the staining solution for 1 hour prior to imaging. For imaging of whole pancreas

explants, *Il13*$^{tdTom/+}$*Foxp3*$^{YFP\text{-}Cre}$ mice were injected with 200 ng rmIL-33 intraperitoneally for 2 days and sacrificed 3 days after the first injection. One day prior to sacrifice, mice were injected intraperitoneally with Hoechst 33342 (Thermo Scientific). PCLS and pancreas explants were imaged on an inverted laser-scanning confocal microscope (Stellaris 8, Leica Microsystems) with an attached pulsed Coherent Chameleon Ultra II laser, using a 25X 0.95NA water immersion objective lens. Hoechst and tdTomato were excited at a 2-photon excitation wavelengths of 800 nm and 1040nm, respectively. YFP and AF647 were excited at single-photon excitation wavelengths of 488nm and 633nm, respectively.

Multiplex immunofluorescence imaging was performed on formalin-fixed paraffin-embedded lung sections using Opal multiplex IHC kits (Akoya Biosciences), following manufacturer instructions. Antigen retrieval was performed using 10mM sodium citrate (pH 6) and sections were stained using primary antibodies against Gata3 (abcam, ab199428), CD3 (abcam, ab11089), and Foxp3 (Thermo Scientific, 14-5773-82). After washing, sections were incubated with HRP-conjugated anti-rabbit (Akoya Biosciences) or anti-rat (abcam, ab214882) polymer-HRP secondary antibody for 15 minutes. The Opal Polaris 480, Opal 570, and Opal 690 reagents were used for visualisation of Gata3, Foxp3, and CD3 respectively.

Stained multiplex immunofluorescence sections were imaged on an inverted laser-scanning confocal microscope (Stellaris 8, Leica Microsystems) using a 25X 0.95NA water immersion objective lens. Large sections of tissue were imaged for downstream analysis as a maximum intensity projection (typically a z-stack of 10 µm, 40-60 tiles). Image analysis was performed using the HALO software (Indica Labs). Cell types were identified using the HighPlex-FL algorithm, and fine-tuned for cell types of interest detailed in the main text.

Bulk RNAseq

Treg ($CD45^+CD3^+CD4^+CD8^-TCR\beta^+YFP^+$) and Tconv ($CD45^+CD3^+CD4^+CD8^-TCR\beta^+YFP^-$) cells were sorted from spleens of *Foxp3*$^{YFP\text{-}Cre}$*Tnfrsf4*$^{fl/fl}$ mice using a BD Aria II cell sorter. $Gata3^{high}$ and $Gata3^{low}$ Treg cells ($CD45^+Lin^-CD3^+CD8^-TCR\beta^+CD4^+RFP^+YFP^{hi/lo}$), Tconv and Th2 cells ($CD45^+Lin^-CD3^+CD8^-TCR\beta^+CD4^+RFP^-YFP^{lo/hi}$) and ILC2s ($CD45^+Lin^-CD3^-CD4^-YFP^{hi}$) were sorted from lungs of IL-33-sensitised *Gata3*$^{YFP/YFP}$*Foxp3*^{RFP} mice on a BD Symphony S6 sorter.

RNA was extracted using RNeasy plus micro kit (Qiagen) and 5 to 15 ng used as input material for library preparation. Libraries were generated with the NEBNext® Single Cell/Low Input RNA Library Prep Kit for Illumina (NEB) according to manufacturer's instructions. The pooled

libraries were quantified with KAPA Library Quantification Kit for Illumina (Kapa Biosystems) and sequenced (paired end 150nt) on an Illumina NovaSeq 6000 system (Illumina).

Bulk RNA-seq analysis

The quality of raw sequence data was assessed using FastQC (v 0.11.9). Raw sequence was trimmed for adapter content using Trimmomatic (v 0.39) and aligned to the GRCm38.p6 genome using STAR (v 2.7.7a). Alignment quality was assess using Picard's CollectAlignmentMetrics, CollectRnaSeqMetrics, MarkDuplicates and CollectInsertSizeMetrics tools (v 2.25.1 for the spleen dataset and v 2.27.3 for the lung dataset). Quantification of gene expression was performed using Salmon (v 1.6.0 for the spleen dataset and v 1.9.0 for the lung dataset) in mapping-based mode versus the Ensembl release 102 transcriptome. Differential gene expression analysis was carried out using DESeq2 (v 1.34.0) in R (v 4.1.2). For the spleen dataset, batch effects between the two sequencing pools were accounted for by including the sequencing pool as a term in the linear model. The effectiveness of this strategy was confirmed using the `removeBatchEffect` function from the limma package (v 3.50.0) to generate a batch corrected counts matrix, followed by principal component analysis to assess remaining batch effects.

In the spleen dataset, 2 KO samples were excluded based on high *Tnfrsf4* expression, indicating mis-genotyping, and 3 poor quality samples were excluded based on low read counts. In the lung dataset, 2 ILC2 samples were excluded based on high *Foxp3* expression, indicating contamination of the sorted cells with Tregs.

Heatmaps were drawn using pheatmap (v 1.0.12), and gene set enrichment analyses were performed using clusterProfiler (v 4.4.4) and gene set collection C7 (Immunological signatures, including the gene set GSE7852_TREG_VS_TCONV_FAT_UP[67]) in R. We used CellChat[27] to predict putative cell-cell communication pathways. As CellChat was developed for use in single-cell applications, we instead defined over-expressed genes as genes for which at least one sample has a normalised expression count exceeding 1000. Computation of communication probability was also performed using the 'truncatedMean' method, with trim=0.1.

TCR sequences analysis were extracted from RNA-seq data using MiXCR (v 4.0.0). Diversity metrics along with abundance analyses were carried out with the Immunarch package (v 0.8.0) in R.

Statistics

Analysis for two groups were calculated using an unpaired two-tailed Student's *t*-test; comparisons of more than two groups were calculated using a one-way analysis of variance (ANOVA) with Tukey post-analysis. All data were analysed using GraphPad Prism 9 (GraphPad Software) except for the histology scores, which were analysed using a permutation test in R (*perm.test* function of the R package *exactRankTests*). Results with $p \leq 0.05$ being considered significant (*), $p \leq 0.01$ = **, $p \leq 0.001$ = ***, $p \leq 0.0001$ = ****.

DATA AND SOFTWARE AVAILABILITY

Sequencing data have been deposited under the accession number GSE230599.

Figures and Figure Legends

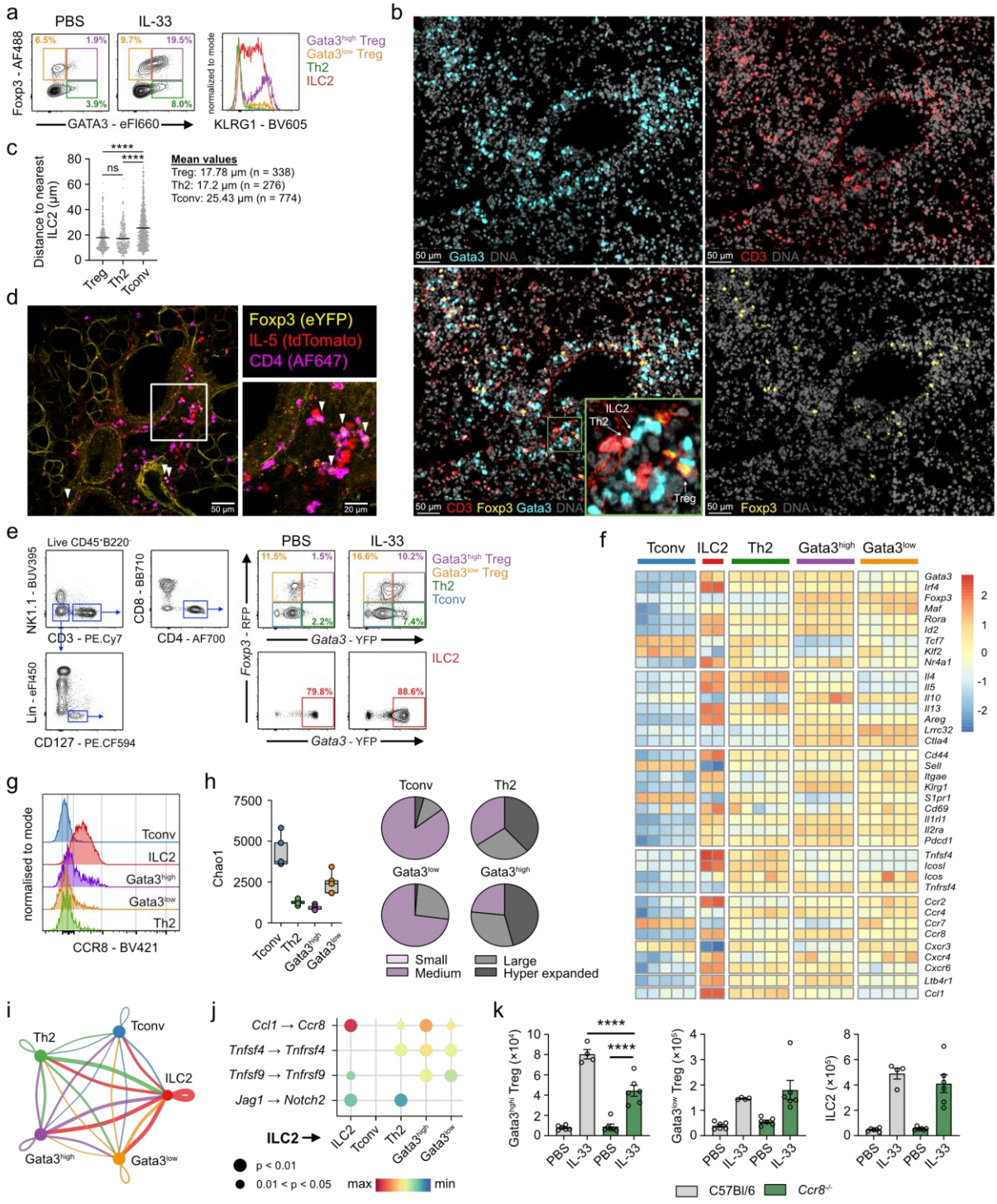

Figure 1. Type-2 effector and regulatory lymphocytes express gene-signatures that enforce localisation and enable crosstalk mechanism in the inflamed lung niche.

PBS and IL-33-treated wild-type lungs were analysed for the indicated $CD4^+$ T cell subsets (pre-gated on $CD3^+CD4^+CD8^-NK1.1^-B220^-CD45^+$ live cells) (*left*) and expression of KLRG1 on the indicated cell-types (*right*) (**a**). Multiplex IF microscopy of IL-33-treated lung sections

allowed the identification of $CD3^+Foxp3^-Gata3^-$ Tconv, $CD3^+Foxp3^-Gata3^+$ Th2, $CD3^+Foxp3^+$ Treg and $CD3^-Foxp3^-Gata3^+$ ILC2 (**b**), followed by automated analysis of distances between the indicated cell-types (**c**). ILC2 (*Il5*$^{tdTom+}$$CD4^-$) and Tregs (*Foxp3*$^{YFP+}$$CD4^+$) were visualised in lung sections of IL-33-treated *Il5*$^{tdTom/+}$*Foxp3*$^{YFP/y}$ mice (**d**).

e-k. *Gata3*^{YFP}*Foxp3*^{RFP} mouse lungs were used to identify $CD4^+$ T cell-subsets and ILC2 in PBS and IL-33 treated lungs (**e**). Bulk RNA-seq data of the indicated populations (top row), flow-sorted from the lungs of *Gata3*^{YFP}*Foxp3*^{RFP} reporter mice after IL-33 administration on day 0 and 1, followed by sacrifice on day 5 (**f**), and cell-surface CCR8 expression on the indicated populations (**g**). TCR diversity analysis was performed on the transcriptomic data of the indicated T cell populations (left); pie charts show proportions of the indicated clonal subgroups (right) in the indicated T cell populations (**h**). CellChat analysis was performed on the indicated populations to predict homotypic and heterotypic interactions; colour of the lines represent direction (i.e. ligand expression by same colour cell), while width represents the number of interactions (**i**). Several interactions whereby ILC2 were predicted to engage themselves, or the indicated T cell population (bottom axis). (**j**). Wild-type or *Ccr8*$^{-/-}$ mice were treated with PBS or IL-33 on days 0 and 1, followed by quantification of the indicated populations in the airways on day 5 (**k**).

Microscopy images are representative of 2(**b**) or 3(**d**) independent experiments. Histogram images are representative of >3(**a**) or 2(**g**) independent experiments. Bar graphs indicate mean (±SEM) (n=5,5,5,5; **c**) and show representative data of two independent experiments in (**c**) and (n=6,4,6,6; **k**). ns = not significant, **** = $p \leq 0.0001$.

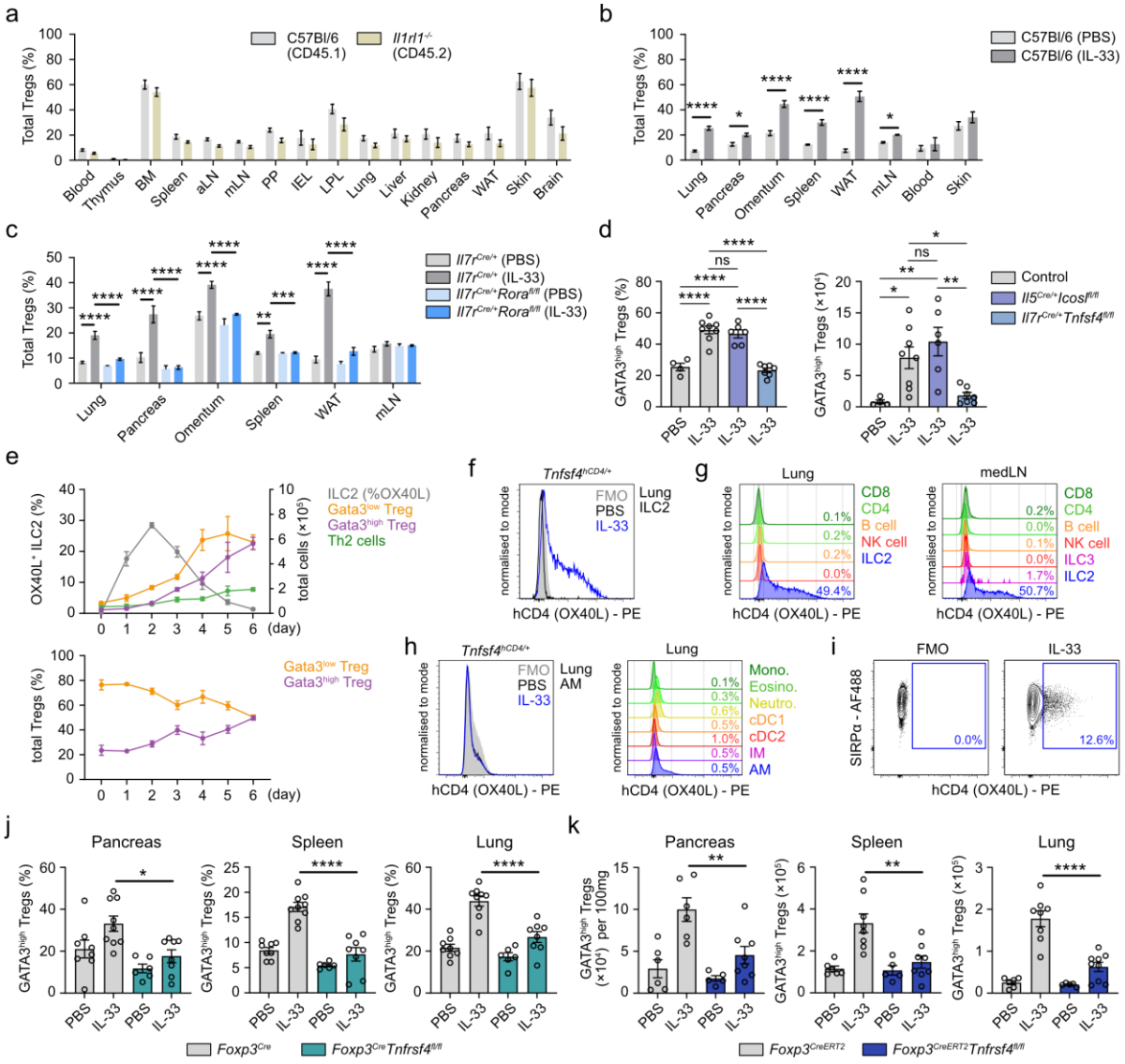

Figure 2. ILC2 and the OX40L-OX40 signalling axis control tissue-specific Gata3^{high} Treg responses to IL-33.

Donor derived wild-type (C57Bl/6) and *Il1rl1*$^{-/-}$ Tregs were quantified in the indicated tissues of untreated (50:50, WT/KO) bone marrow chimeric mice (**a**). Tregs were quantified in the indicated tissues of PBS or IL-33-treated (500 ng i/p on day 0 and 1, tissue collection on day 5) wild-type mice (**b**), and *Il7r*$^{Cre/+}$ or *Il7r*$^{Cre/+}$*Rora*$^{fl/fl}$ mice (**c**). Lung Gata3^{high} Tregs were quantified in PBS or IL-33 treated (200 ng i/n on day 0 and 1, tissue collection on day 5) mice of the indicated genotypes (**d**). Wild-type mice were intranasally dosed with IL-33 on days 0 and 1, followed by the analysis of lungs at the indicated time points to determine OX40L expression by ILC2 (top, left axis) or the total numbers of the indicated cell types (top, right axis) (**e**); the percentage of Gata3^{high} and Gata3^{low} Tregs was measured in the lungs at different time points (bottom).

f-i. *Tnfsf4*$^{hCD4/+}$ mice were treated with IL-33 or PBS (200ng i/n on day 0 and 1, tissue collection on day 3) followed by measurement of hCD4 on lung ILC2 (**f**) and the indicated lymphocytes in the lung and mediastinal lymph node (**g**), the indicated lung myeloid cells (**h**, representative staining on alveolar macrophages shown left), and cDC2 in the medLN (**i**).
j-k. Mice of the indicated genotypes were treated with PBS or IL-33 (500ng i/p) on day 0 and 1, followed by quantification of Gata3^{high} Treg percentages (**j**) and numbers (**k**) in the indicated organs on day 5 (all mice were treated with tamoxifen in **k**).

Dot plots show representative gating strategy; numbers indicate percent of gated cells. Fluorescence minus one (FMO), Bone marrow (BM), axillary (a)LN), mesenteric (m)LN, Peyer's patch (PP), intraepithelial lymphocytes (IEL), lamina propria lymphocytes (LPL), white adipose tissue (WAT). Bar graphs indicate mean (±SEM) and show data of one experiment (n=4 for all; **a**), representative data of 2 independent experiments (n=5,5,4,5,5,5,5,5,5,5,5,5,5,5,5; **b**), or pooled data from 2 independent experiments (n=8,9,7,9,6,8,7,9,7,7,5,6,6,8,7,9,4,4,4,4,4,4 ,4,4; **c**), (n=4,8,6,7; **d**), (n=4 for day 0, 6 for all other days; **e**), (n=8,9,6,8, left; n=8,9,6,8, middle; n=8,9,6,8, right; **j**), (n= 6,6,5,8, left; n=6,8,5,8, middle; n=6,8,5,9, right; **k**) mice per group. ns = not significant, * = $p \leq 0.05$, ** = $p \leq 0.01$, *** = $p \leq 0.001$, **** = $p \leq 0.0001$.

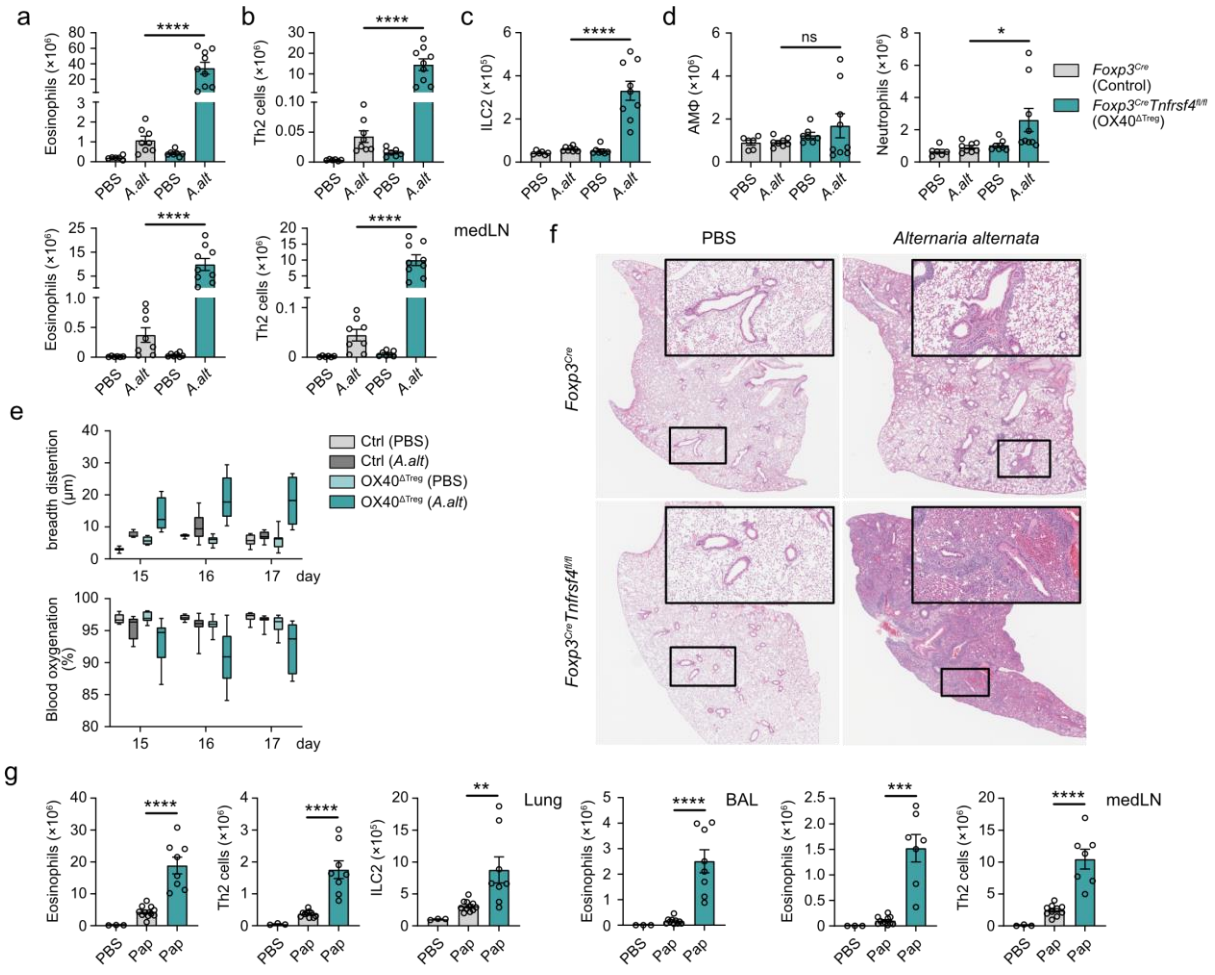

Figure 3. Treg-intrinsic OX40 is critical for the effective control of type-2 inflammation.

a-f. Mice of the indicated genotypes were treated intranasally with *Alternaria alternata* or PBS on days 0, 1 and 14, followed by sacrifice on day 20. Flow cytometric quantification of lung (top) and medLN (bottom) eosinophil (**a**) and Th2 cell numbers (**b**). Flow cytometric quantification of ILC2 (**c**) and alveolar macrophage (left) and neutrophil (right) cell numbers (**d**). Mice were analysed by pulse oximetry for breadth distention (top) and blood oxygenation (bottom) on the indicated days (**e**). Representative H&E staining of lung sections (**f**).

g. Mice were treated intranasally with papain or PBS on days 0, 1 and 14, followed by sacrifice on day 20. Flow cytometric quantification of lung eosinophil, Th2 and ILC2 cell numbers (left), BAL eosinophil cell numbers (middle), and medLN eosinophil and Th2 cell numbers (right).

Representative histology images shown of 2 independent experiments. Bar graphs indicate mean (±SEM) and show combined data of 2 independent experiments with (n=6,8,7,9; **a-e**) and (n=3,10,8; **g**) mice per group. * = p ≤ 0.05, ** = p ≤ 0.01, *** = p ≤ 0.001, **** = p ≤ 0.0001.

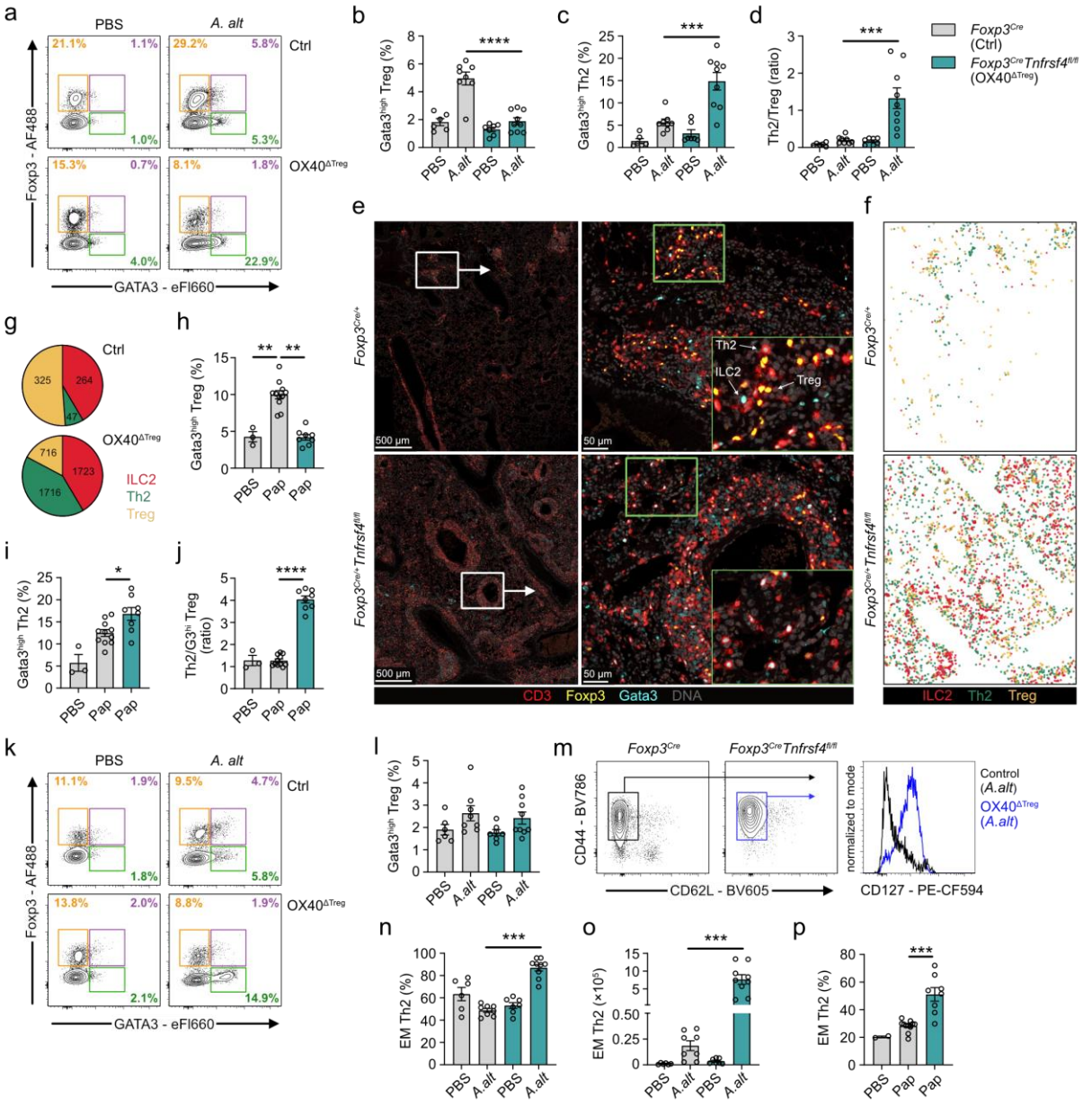

Figure 4. Allergen exposed OX40$^{\Delta Treg}$ mice have impaired Gata3^{high} Treg induction and amplified effector memory Th2 cell expansion.

a-g. The lungs of PBS- or *Alternaria alternata*-treated mice of the indicated genotypes were analysed for percentages of Gata3^{low} and Gata3^{high} Tregs (yellow and purple), or Th2 cells (green) by flow cytometry (representative dot plots in **a**, treated i/n on day 0, 1 and 14, sacrificed on day 20), followed by quantification of the percentage of Gata3^{high} Tregs (**b**) and Th2 cells (**c**) or indicated cell ratios (**d**). Multiplex IF microscopy of lung sections allowed the identification of CD3^{+}Foxp3^{-}Gata3^{+} Th2, CD3^{+}Foxp3^{+} Treg and CD3^{-}Foxp3^{-}Gata3^{+} ILC2 (**e**), followed by automated analysis of cell-type densities using HALO (**f, g**).

h-j. The percentage of Gata3^{high} Tregs (**h**) and Th2 cells (**i**) or indicated cell ratios (**j**) were measured in the lungs *Foxp3^{Cre}* or *Foxp3^{Cre}Tnfrsf4$^{fl/fl}$* mice treated with PBS or papain (same dosing as in a).

k-p. The medLN of PBS, *Alternaria alternata* or papain treated mice of the indicated genotypes were analysed for percentages of Gata3^{low} and Gata3^{high} Tregs (yellow and purple), or Th2 cells (green) by flow cytometry (**k**). The percentages of Gata3^{high} Tregs (% of total CD4^{+}) were measured (**l**). Th2 cells were further analysed for expression of CD127 on CD44^{+}CD62L^{-} cells (**m**), followed by measurement of CD44^{+}CD62L^{-}CD127^{+} effector memory (EM) Th2 cell percentages (**n**) and numbers (**o**). Similarly, EM Th2 cell percentages (% of Th2) were measured in PBS and papain-treated mice (**p**).

Dot plots show representative gating strategy; numbers indicate percent of gated cells. Bar graphs indicate mean (±SEM) and show combined data of 2 independent experiments with (n=6,8,7,9; **b-d**, **i**, **k**, **l**) and (n=3,10,8; **e-g**, **m**) mice per group. * = $p \leq 0.05$, ** = $p \leq 0.01$, *** = $p \leq 0.001$, **** = $p \leq 0.0001$.

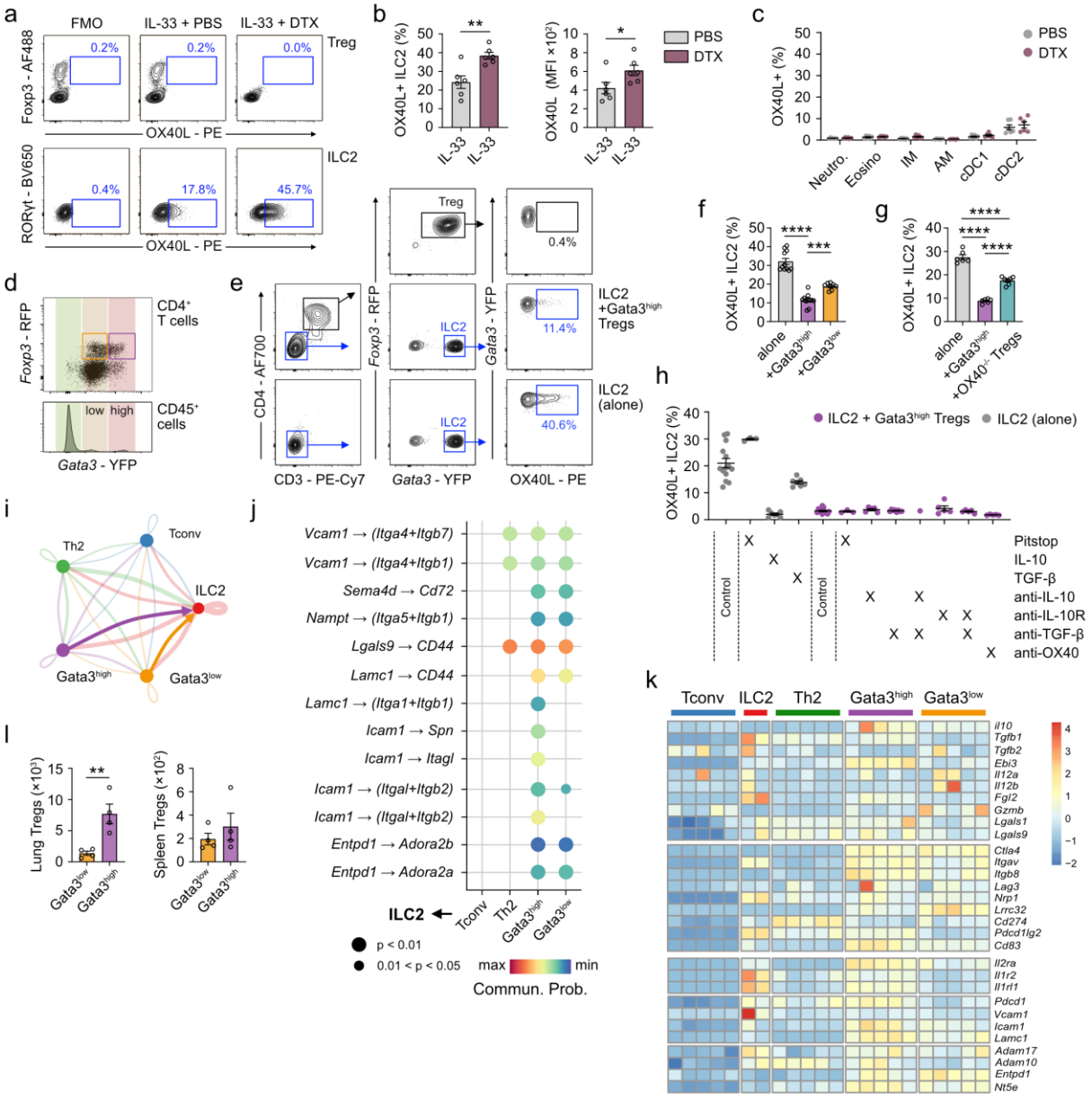

Figure 5. Gata3^{high} Tregs directly control OX40L availability on ILC2 and preferentially home to the inflamed lung.

a-c. *Foxp3^{DTR}* mice were treated intranasally with IL-33 plus *diphtheria* toxin (DTX) or PBS on days 0, and 1, and sacrificed on day 3. Representative flow cytometric identification of OX40L^{+} lung Treg and ILC2 cells (**a**), and quantification of OX40L^{+} ILC2 cells expressed as percentage (left) and mean fluorescence intensity (right) (**b**), and percent OX40L^{+} myeloid cells (**c**).

d-h. Gata3^{high} (purple) or Gata3^{low} (orange) Tregs were identified and flow sorted alongside ILC2 from *Gata3^{YFP}Foxp3^{RFP}* mouse lungs (**d**, *see also Supplemental Figure 1d*); ILC2 were co-cultured alone or with the indicated Treg populations for 20 hours followed by measurement of OX40L expression on ILC2 or Tregs by flow cytometry (**e** shows representative gating, **f** show percent OX40L^{+} ILC2 for each condition). OX40-deficient Tregs were flow-sorted from

Foxp3^{Cre}*Tnfrsf4*$^{fl/fl}$ mice and compared with Gata3^{high} Tregs in their ability to suppress OX40L on ILC2 (**g**). ILC2 monocultures (grey) or Gata3^{high} Treg co-cultures (purple) were supplemented with the indicated reagents, followed by measurement of OX40L expression on ILC2 (**h**).

i-k. Computational analysis using CellChat of Treg-to-ILC2 interactions (**i**) revealed several pathways that were selectively enriched or present in Gata3^{high} Tregs (**j**).

Gata3^{high} or Gata3^{low} Tregs were flow-sorted from IL-33-treated *Gata3*^{YFP}*Foxp3*^{RFP} mouse lungs followed by adoptive transfer of 2.5×10^3 cells into *Rag2*$^{-/-}$ recipient mice. Two days later the lungs and spleens of recipient mice were analysed for numbers of Foxp3^{RFP+} Tregs (**l**).

Dot plots show representative gating strategy; numbers indicate percent of gated cells. Bar graphs indicate mean (±SEM) and show combined data of 2 (b, f), or 3 (e, g) independent experiments with (n=6,6; b) or (n=4,4; g) mice or (n=11,11,8; e) or (n=6,6,7; f) co-culture experiments per group. ** = $p \leq 0.01$, *** = $p \leq 0.001$, **** = $p \leq 0.0001$.

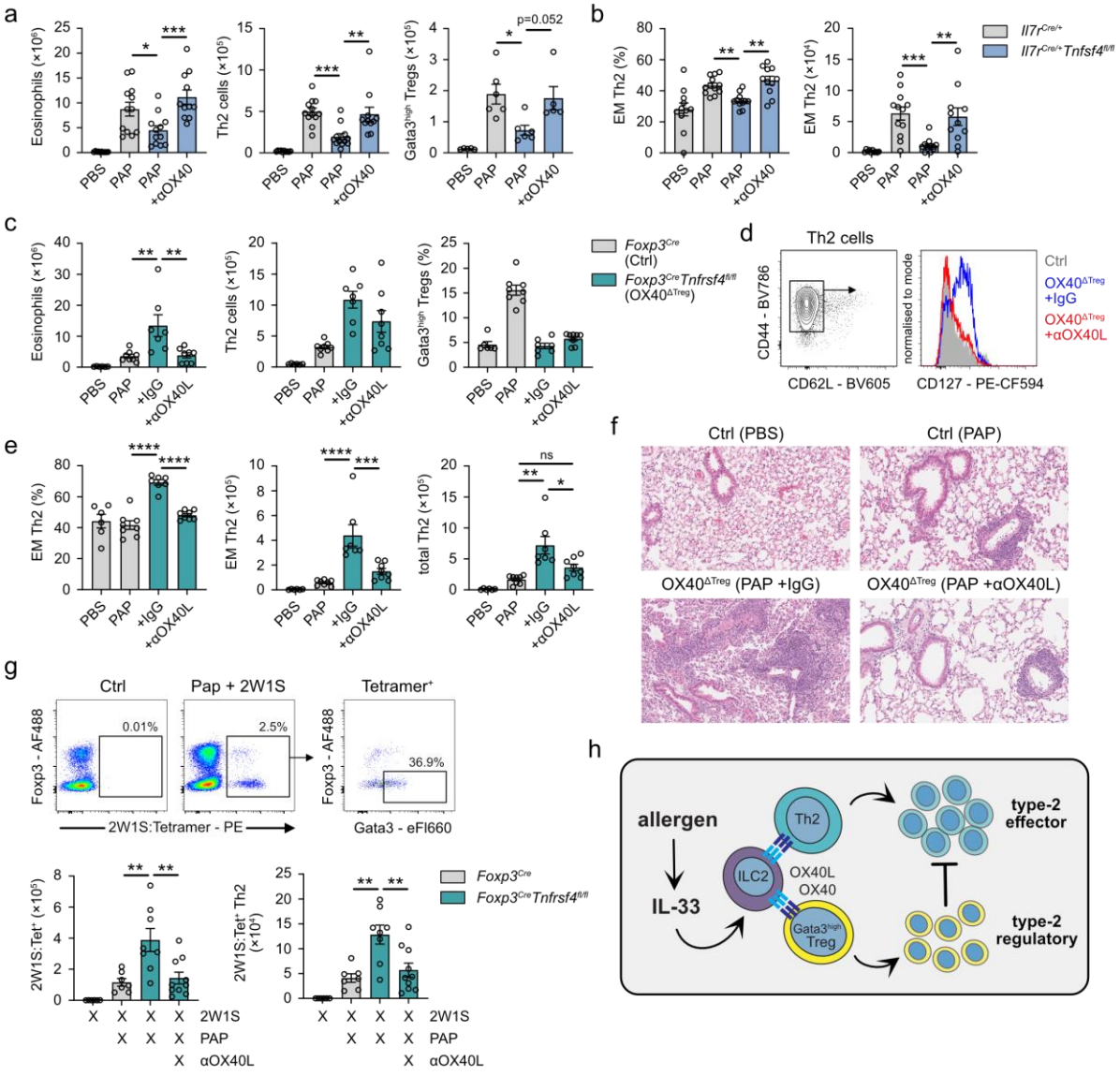

Figure 6. OX40⁺ Tregs control adaptive type-2 immunity by modulating OX40L availability.

a-b. Mice of the indicated genotypes were treated intranasally with PBS or papain on days 0, 1 and 14, plus OX40 agonist (mouse IgG1) as indicated (*see Supplemental Figure 7a*) followed by sacrifice on day 20. Flow cytometric quantification of lung eosinophil, Th2 cell and Gata3^{high} Treg cell numbers (**a**). medLN effector memory Th2 percentage (left) and numbers (right) were measured (**b**).

c-f. Mice of the indicated genotypes were treated intranasally with PBS or papain on days 0, 1 and 14, plus anti-OX40L or rat IgG isotype control as indicated (*see Supplemental Figure 7b*) followed by sacrifice on day 20. Flow cytometric quantification of lung eosinophil, total Th2 cell and Gata3^{high} Treg cell numbers (**c**). Representative flow cytometric identification (**d**) and

quantification (**e**) of total medLN EM Th2 (left and middle) or total Th2 (right) cells. Representative H&E staining of lung sections (**f**).

g. Mice were treated intranasally with PBS (+2W1S peptide) or papain (+2W1S peptide) on days 0, 1 and 14, plus anti-OX40L as indicated (*see Supplemental Figure 7b*) followed by sacrifice on day 20. 2W1S:tetramer-positive $CD4^+$ cells were detected by flow cytometry (PBS + 2W1S and papain + 2W1S treated *Foxp3*^{Cre} control mice shown, left), followed by intracellular detection of Foxp3 and Gata3 (right) (**g**, top) 2W1S:tetramer$^+$ total (left) and Th2 (right) cells were quantified in the lungs of mice treated as indicated (**g**, bottom).

h. Graphical abstract.

Representative histology images shown of 2 independent experiments. Dot plots show representative gating strategy; numbers indicate percent of gated cells. Bar graphs indicate mean (±SEM) and show combined or representative data of two independent experiments with (n=11,12,12,11; **a-b**, n=5,6,6,5; right panel of **a**), (n=6,8,7,8; **c**, **e**) and (n=6,7,8,10; **g**) mice per group. ns = not significant, * = $p \leq 0.05$, ** = $p \leq 0.01$, *** = $p \leq 0.001$, **** = $p \leq 0.0001$.

References

1. Meizlish, M.L., Franklin, R.A., Zhou, X., and Medzhitov, R. (2021). Tissue Homeostasis and Inflammation. Annu. Rev. Immunol. *39*, 557–581.

2. Dikiy, S., and Rudensky, A.Y. (2023). Principles of regulatory T cell function. Immunity *56*, 240–255.

3. Powell, B.R., Buist, N.R.M., and Stenzel, P. (1982). An X-linked syndrome of diarrhea, polyendocrinopathy, and fatal infection in infancy. J. Pediatr. *100*, 731–737.

4. Lahl, K., Mayer, C.T., Bopp, T., Huehn, J., Loddenkemper, C., Eberl, G., Wirnsberger, G., Dornmair, K., Geffers, R., Schmitt, E., et al. (2009). Nonfunctional regulatory T cells and defective control of Th2 cytokine production in natural scurfy mutant mice. J. Immunol. *183*, 5662–5672.

5. Chatila, T.A., Blaeser, F., Ho, N., Lederman, H.M., Voulgaropoulos, C., Helms, C., and Bowcock, A.M. (2000). JM2, encoding a fork head-related protein, is mutated in X-linked autoimmunity-allergic disregulation syndrome. J. Clin. Invest. *106*, R75-81.

6. Zheng, Y., Chaudhry, A., Kas, A., deRoos, P., Kim, J.M., Chu, T.-T., Corcoran, L., Treuting, P., Klein, U., and Rudensky, A.Y. (2009). Regulatory T-cell suppressor program co-opts transcription factor IRF4 to control T(H)2 responses. Nature *458*, 351–356.

7. Wohlfert, E.A., Grainger, J.R., Bouladoux, N., Konkel, J.E., Oldenhove, G., Ribeiro, C.H., Hall, J.A., Yagi, R., Naik, S., Bhairavabhotla, R., et al. (2011). GATA3 controls Foxp3$^+$ regulatory T cell fate during inflammation in mice. J. Clin. Invest. *121*, 4503–4515.

8. Koch, M.A., Tucker-Heard, G., Perdue, N.R., Killebrew, J.R., Urdahl, K.B., and Campbell, D.J. (2009). The transcription factor T-bet controls regulatory T cell homeostasis and function during type 1 inflammation. Nat. Immunol. *10*, 595–602.

9. Littman, D.R., and Rudensky, A.Y. (2010). Th17 and regulatory T cells in mediating and restraining inflammation. Cell *140*, 845–858.

10. Turner, J.-E., Paust, H.-J., Steinmetz, O.M., Peters, A., Riedel, J.-H., Erhardt, A., Wegscheid, C., Velden, J., Fehr, S., Mittrücker, H.-W., et al. (2010). CCR6 recruits regulatory T cells and Th17 cells to the kidney in glomerulonephritis. J. Am. Soc. Nephrol. *21*, 974–985.

11. Singh, R., Alape, D., de Lima, A., Ascanio, J., Majid, A., and Gangadharan, S.P. (2019). Regulatory T Cells in Respiratory Health and Diseases. Pulm. Med. *2019*, 1907807.

12. Bacher, P., Heinrich, F., Stervbo, U., Nienen, M., Vahldieck, M., Iwert, C., Vogt, K., Kollet, J., Babel, N., Sawitzki, B., et al. (2016). Regulatory T Cell Specificity Directs Tolerance versus Allergy against Aeroantigens in Humans. Cell *167*, 1067-1078.e16.

13. Bacher, P., and Scheffold, A. (2018). The effect of regulatory T cells on tolerance to airborne allergens and allergen immunotherapy. J. Allergy Clin. Immunol. *142*, 1697–1709.

14. Schiering, C., Krausgruber, T., Chomka, A., Fröhlich, A., Adelmann, K., Wohlfert, E.A., Pott, J., Griseri, T., Bollrath, J., Hegazy, A.N., et al. (2014). The alarmin IL-33 promotes regulatory T-cell function in the intestine. Nature *513*, 564–568.

15. Faustino, L.D., Griffith, J.W., Rahimi, R.A., Nepal, K., Hamilos, D.L., Cho, J.L., Medoff, B.D., Moon, J.J., Vignali, D.A.A., and Luster, A.D. (2020). Interleukin-33 activates regulatory T cells to suppress innate γδ T cell responses in the lung. Nat. Immunol. *21*, 1371–1383.

16. Kolodin, D., van Panhuys, N., Li, C., Magnuson, A.M., Cipolletta, D., Miller, C.M., Wagers, A., Germain, R.N., Benoist, C., and Mathis, D. (2015). Antigen- and cytokine-driven accumulation of regulatory T cells in visceral adipose tissue of lean mice. Cell Metab. *21*, 543–557.

17. Vasanthakumar, A., Moro, K., Xin, A., Liao, Y., Gloury, R., Kawamoto, S., Fagarasan, S., Mielke, L.A., Afshar-Sterle, S., Masters, S.L., et al. (2015). The transcriptional regulators IRF4, BATF and IL-33 orchestrate development and maintenance of adipose tissue–resident regulatory T cells. Nat. Immunol. *16*, 276–285.

18. Kuswanto, W., Burzyn, D., Panduro, M., Wang, K.K., Jang, Y.C., Wagers, A.J., Benoist, C., and Mathis, D. (2016). Poor Repair of Skeletal Muscle in Aging Mice Reflects a Defect in Local, Interleukin-33-Dependent Accumulation of Regulatory T Cells. Immunity *44*, 355–367.

19. Halim, T.Y.F., Rana, B.M.J., Walker, J.A., Kerscher, B., Knolle, M.D., Jolin, H.E., Serrao, E.M., Haim-Vilmovsky, L., Teichmann, S.A., Rodewald, H.-R., et al. (2018). Tissue-Restricted Adaptive Type 2 Immunity Is Orchestrated by Expression of the Costimulatory Molecule OX40L on Group 2 Innate Lymphoid Cells. Immunity *48*, 1195-1207.e6.

20. Molofsky, A.B., Van Gool, F., Liang, H.-E., Van Dyken, S.J., Nussbaum, J.C., Lee, J., Bluestone, J.A., and Locksley, R.M. (2015). Interleukin-33 and Interferon-γ Counter-Regulate Group 2 Innate Lymphoid Cell Activation during Immune Perturbation. Immunity *43*, 161–174.

21. Hemmers, S., Schizas, M., and Rudensky, A.Y. (2021). T reg cell-intrinsic requirements for ST2 signaling in health and neuroinflammation. J. Exp. Med. *218*. 10.1084/jem.20201234.

22. Rao, T.N., Kumar, S., Pulikkottil, A.J., Oliveri, F., Hendriks, R.W., Beckel, F., and Fehling, H.J. (2020). Novel, Non-Gene-Destructive Knock-In Reporter Mice Refute the Concept of Monoallelic Gata3 Expression. J. Immunol. *204*, 2600–2611.

23. Faustino, L., Mucida, D., Keller, A.C., Demengeot, J., Bortoluci, K., Sardinha, L.R., Carla Takenaka, M., Basso, A.S., Faria, A.M.C., and Russo, M. (2012). Regulatory T cells accumulate in the lung allergic inflammation and efficiently suppress T-cell proliferation but not Th2 cytokine production. Clin. Dev. Immunol. *2012*, 721817.

24. Mikhak, Z., Fukui, M., Farsidjani, A., Medoff, B.D., Tager, A.M., and Luster, A.D. (2009). Contribution of CCR4 and CCR8 to antigen-specific T(H)2 cell trafficking in allergic pulmonary inflammation. J. Allergy Clin. Immunol. *123*, 67-73.e3.

25. Sather, B.D., Treuting, P., Perdue, N., Miazgowicz, M., Fontenot, J.D., Rudensky, A.Y., and Campbell, D.J. (2007). Altering the distribution of Foxp3+ regulatory T cells results in tissue-specific inflammatory disease. J. Exp. Med. *204*, 1335–1347.

26. Obata-Ninomiya, K., Ishiwata, K., Nakano, H., Endo, Y., Ichikawa, T., Onodera, A., Hirahara, K., Okamoto, Y., Kanuka, H., and Nakayama, T. (2018). $CXCR6^{+}ST2^{+}$ memory T helper 2 cells induced the expression of major basic protein in eosinophils to reduce

the fecundity of helminth. Proceedings of the National Academy of Sciences *115*, E9849–E9858.

27. Jin, S., Guerrero-Juarez, C.F., Zhang, L., Chang, I., Ramos, R., Kuan, C.-H., Myung, P., Plikus, M.V., and Nie, Q. (2021). Inference and analysis of cell-cell communication using CellChat. Nat. Commun. *12*, 1–20.

28. Knipfer, L., Schulz-Kuhnt, A., Kindermann, M., Greif, V., Symowski, C., Voehringer, D., Neurath, M.F., Atreya, I., and Wirtz, S. (2019). A CCL1/CCR8-dependent feed-forward mechanism drives ILC2 functions in type 2-mediated inflammation. J. Exp. Med. *216*, 2763–2777.

29. Wang, Y., Su, M.A., and Wan, Y.Y. (2011). An essential role of the transcription factor GATA-3 for the function of regulatory T cells. Immunity *35*, 337–348.

30. Van Dyken, S.J., Nussbaum, J.C., Lee, J., Molofsky, A.B., Liang, H.-E., Pollack, J.L., Gate, R.E., Haliburton, G.E., Ye, C.J., Marson, A., et al. (2016). A tissue checkpoint regulates type 2 immunity. Nat. Immunol. *17*, 1381–1387.

31. Halim, T.Y.F., Hwang, Y.Y., Scanlon, S.T., Zaghouani, H., Garbi, N., Fallon, P.G., and McKenzie, A.N.J. (2016). Group 2 innate lymphoid cells license dendritic cells to potentiate memory TH2 cell responses. Nat. Immunol. *17*, 57–64.

32. Halim, T.Y.F., Krauss, R.H., Sun, A.C., and Takei, F. (2012). Lung natural helper cells are a critical source of Th2 cell-type cytokines in protease allergen-induced airway inflammation. Immunity *36*, 451–463.

33. Cayrol, C., Duval, A., Schmitt, P., Roga, S., Camus, M., Stella, A., Burlet-Schiltz, O., Gonzalez-de-Peredo, A., and Girard, J.-P. (2018). Environmental allergens induce allergic inflammation through proteolytic maturation of IL-33. Nat. Immunol. *19*, 375–385.

34. Gramaglia, I., Jember, A., Pippig, S.D., Weinberg, A.D., Killeen, N., and Croft, M. (2000). The OX40 costimulatory receptor determines the development of CD4 memory by regulating primary clonal expansion. J. Immunol. *165*, 3043–3050.

35. Rigas, D., Lewis, G., Aron, J.L., Wang, B., Banie, H., Sankaranarayanan, I., Galle-Treger, L., Maazi, H., Lo, R., Freeman, G.J., et al. (2017). Type 2 innate lymphoid cell suppression by regulatory T cells attenuates airway hyperreactivity and requires inducible T-cell costimulator–inducible T-cell costimulator ligand interaction. J. Allergy Clin. Immunol. *139*, 1468-1477.e2.

36. Croft, M. (2010). Control of Immunity by the TNFR-Related Molecule OX40 (CD134). Annu. Rev. Immunol. *28*, 57–78.

37. Deng, T., Suo, C., Chang, J., Yang, R., Li, J., Cai, T., and Qiu, J. (2020). ILC3-derived OX40L is essential for homeostasis of intestinal Tregs in immunodeficient mice. Cell. Mol. Immunol. *17*, 163–177.

38. Jenkins, S.J., Perona-Wright, G., Worsley, A.G.F., Ishii, N., and MacDonald, A.S. (2007). Dendritic cell expression of OX40 ligand acts as a costimulatory, not polarizing, signal for optimal Th2 priming and memory induction in vivo. J. Immunol. *179*, 3515–3523.

39. Lyu, M., Suzuki, H., Kang, L., Gaspal, F., Zhou, W., Goc, J., Zhou, L., Zhou, J., Zhang, W., Shen, Z., et al. (2022). ILC3s select microbiota-specific regulatory T cells to establish tolerance in the gut. Nature *610*, 744–751.

40. Halim, T.Y.F., Steer, C.A., Mathä, L., Gold, M.J., Martinez-Gonzalez, I., McNagny, K.M., McKenzie, A.N.J., and Takei, F. (2014). Group 2 innate lymphoid cells are critical for the initiation of adaptive T helper 2 cell-mediated allergic lung inflammation. Immunity *40*, 425–435.

41. Kedmi, R., Najar, T.A., Mesa, K.R., Grayson, A., Kroehling, L., Hao, Y., Hao, S., Pokrovskii, M., Xu, M., Talbot, J., et al. (2022). A RORγt+ cell instructs gut microbiota-specific Treg cell differentiation. Nature *610*, 737–743.

42. Zhou, L., Chu, C., Teng, F., Bessman, N.J., Goc, J., Santosa, E.K., Putzel, G.G., Kabata, H., Kelsen, J.R., Baldassano, R.N., et al. (2019). Innate lymphoid cells support regulatory T cells in the intestine through interleukin-2. Nature *568*, 405–409.

43. Zhu, J., Yamane, H., and Paul, W.E. (2010). Differentiation of effector CD4 T cell populations (*). Annu. Rev. Immunol. *28*, 445–489.

44. Siegmund, K., Feuerer, M., Siewert, C., Ghani, S., Haubold, U., Dankof, A., Krenn, V., Schön, M.P., Scheffold, A., Lowe, J.B., et al. (2005). Migration matters: regulatory T-cell compartmentalization determines suppressive activity in vivo. Blood *106*, 3097–3104.

45. Yang, B.-H., Hagemann, S., Mamareli, P., Lauer, U., Hoffmann, U., Beckstette, M., Föhse, L., Prinz, I., Pezoldt, J., Suerbaum, S., et al. (2016). Foxp3(+) T cells expressing RORγt represent a stable regulatory T-cell effector lineage with enhanced suppressive capacity during intestinal inflammation. Mucosal Immunol. *9*, 444–457.

46. Sefik, E., Geva-Zatorsky, N., Oh, S., Konnikova, L., Zemmour, D., McGuire, A.M., Burzyn, D., Ortiz-Lopez, A., Lobera, M., Yang, J., et al. (2015). MUCOSAL IMMUNOLOGY. Individual intestinal symbionts induce a distinct population of RORγ^{+} regulatory T cells. Science *349*, 993–997.

47. Nakayama, T., Hieshima, K., Arao, T., Jin, Z., Nagakubo, D., Shirakawa, A.-K., Yamada, Y., Fujii, M., Oiso, N., Kawada, A., et al. (2008). Aberrant expression of Fra-2 promotes CCR4 expression and cell proliferation in adult T-cell leukemia. Oncogene *27*, 3221–3232.

48. Guo, L., Wei, G., Zhu, J., Liao, W., Leonard, W.J., Zhao, K., and Paul, W. (2009). IL-1 family members and STAT activators induce cytokine production by Th2, Th17, and Th1 cells. Proc. Natl. Acad. Sci. U. S. A. *106*, 13463–13468.

49. Siede, J., Fröhlich, A., Datsi, A., Hegazy, A.N., Varga, D.V., Holecska, V., Saito, H., Nakae, S., and Löhning, M. (2016). IL-33 Receptor-Expressing Regulatory T Cells Are Highly Activated, Th2 Biased and Suppress CD4 T Cell Proliferation through IL-10 and TGFβ Release. PLoS One *11*, e0161507.

50. Faustino, L., da Fonseca, D.M., Takenaka, M.C., Mirotti, L., Florsheim, E.B., Guereschi, M.G., Silva, J.S., Basso, A.S., and Russo, M. (2013). Regulatory T cells migrate to airways via CCR4 and attenuate the severity of airway allergic inflammation. J. Immunol. *190*, 2614–2621.

51. Valette, K., Li, Z., Bon-Baret, V., Chignon, A., Bérubé, J.-C., Eslami, A., Lamothe, J., Gaudreault, N., Joubert, P., Obeidat, M., et al. (2021). Prioritization of candidate causal genes for asthma in susceptibility loci derived from UK Biobank. Communications Biology *4*, 1–15.

52. Cunninghame Graham, D.S., Graham, R.R., Manku, H., Wong, A.K., Whittaker, J.C., Gaffney, P.M., Moser, K.L., Rioux, J.D., Altshuler, D., Behrens, T.W., et al. (2008). Polymorphism at the TNF superfamily gene TNFSF4 confers susceptibility to systemic lupus erythematosus. Nat. Genet. *40*, 83–89.

53. Liu, Y., Ke, X., Kang, H.-Y., Wang, X.-Q., Shen, Y., and Hong, S.-L. (2016). Genetic risk of TNFSF4 and FAM167A-BLK polymorphisms in children with asthma and allergic rhinitis in a Han Chinese population. J. Asthma *53*, 567–575.

54. Gutierrez, M., Moreno, V., Heinhuis, K.M., Olszanski, A.J., Spreafico, A., Ong, M., Chu, Q., Carvajal, R.D., Trigo, J., Ochoa de Olza, M., et al. (2021). OX40 Agonist BMS-986178 Alone or in Combination With Nivolumab and/or Ipilimumab in Patients With Advanced Solid Tumors. Clin. Cancer Res. *27*, 460–472.

55. El-Khoueiry, A.B., Spano, J.-P., Angevin, E., Doi, T., Bullock, A.J., Harris, W.P., Hamid, O., Gougis, P., Forgie, A., Yang, W., et al. (2020). Analysis of OX40 agonist antibody (PF-04518600) in patients with hepatocellular carcinoma. J. Clin. Orthod. *38*, 523–523.

56. Webb, G.J., Hirschfield, G.M., and Lane, P.J.L. (2016). OX40, OX40L and Autoimmunity: a Comprehensive Review. Clin. Rev. Allergy Immunol. *50*, 312–332.

57. Kim, J.M., Rasmussen, J.P., and Rudensky, A.Y. (2007). Regulatory T cells prevent catastrophic autoimmunity throughout the lifespan of mice. Nat. Immunol. *8*, 191–197.

58. Rubtsov, Y.P., Rasmussen, J.P., Chi, E.Y., Fontenot, J., Castelli, L., Ye, X., Treuting, P., Siewe, L., Roers, A., Henderson, W.R., Jr, et al. (2008). Regulatory T cell-derived interleukin-10 limits inflammation at environmental interfaces. Immunity *28*, 546–558.

59. Rubtsov, Y.P., Niec, R.E., Josefowicz, S., Li, L., Darce, J., Mathis, D., Benoist, C., and Rudensky, A.Y. (2010). Stability of the regulatory T cell lineage in vivo. Science *329*, 1667–1671.

60. Wan, Y.Y., and Flavell, R.A. (2005). Identifying Foxp3-expressing suppressor T cells with a bicistronic reporter. Proc. Natl. Acad. Sci. U. S. A. *102*, 5126–5131.

61. Nussbaum, J.C., Van Dyken, S.J., von Moltke, J., Cheng, L.E., Mohapatra, A., Molofsky, A.B., Thornton, E.E., Krummel, M.F., Chawla, A., Liang, H.-E., et al. (2013). Type 2 innate lymphoid cells control eosinophil homeostasis. Nature *502*, 245–248.

62. Cortini, A., Ellinghaus, U., Malik, T.H., Cunninghame Graham, D.S., Botto, M., and Vyse, T.J. (2017). B cell OX40L supports T follicular helper cell development and contributes to SLE pathogenesis. Ann. Rheum. Dis. *76*, 2095–2103.

63. Josefowicz, S.Z., Niec, R.E., Kim, H.Y., Treuting, P., Chinen, T., Zheng, Y., Umetsu, D.T., and Rudensky, A.Y. (2012). Extrathymically generated regulatory T cells control mucosal TH2 inflammation. Nature *482*, 395–399.

64. Burich, A., Hershberg, R., Waggie, K., Zeng, W., Brabb, T., Westrich, G., Viney, J.L., and Maggio-Price, L. (2001). Helicobacter-induced inflammatory bowel disease in IL-10- and T cell-deficient mice. Am. J. Physiol. Gastrointest. Liver Physiol. *281*, G764-78.

65. Collison, L.W., and Vignali, D.A.A. (2011). In vitro Treg suppression assays. Methods Mol. Biol. *707*, 21–37.

66. Hu, W., Wang, Z.-M., Feng, Y., Schizas, M., Hoyos, B.E., van der Veeken, J., Verter, J.G., Bou-Puerto, R., and Rudensky, A.Y. (2021). Regulatory T cells function in established systemic inflammation and reverse fatal autoimmunity. Nat. Immunol. *22*, 1163–1174.

67. Feuerer, M., Herrero, L., Cipolletta, D., Naaz, A., Wong, J., Nayer, A., Lee, J., Goldfine, A.B., Benoist, C., Shoelson, S., et al. (2009). Lean, but not obese, fat is enriched for a unique population of regulatory T cells that affect metabolic parameters. Nat. Med. *15*, 930–939.